Performance, Temperature and Concentration Profiles in a Non-Isothermal Ammonia-Fueled Tubular SOFC

by

Nattikarn Jantakananuruk

A Thesis

Submitted to the Faculty

of the

WORCESTER POLYTECHNIC INSTITUTE

In partial fulfillment of the requirements for the

Degree of Master of Science

in

Chemical Engineering

April 2019

APPROVED:

_____

Professor Ravindra Datta, Thesis Advisor

_____

Assistant Professor Andrew R. Teixeira, Thesis Advisor

_____

Professor Nikolaos K. Kazantzis, Thesis Committee Member

_____

Assistant Professor Pratap M. Rao, Thesis Committee Member

Abstract

Ammonia has emerged as an attractive potential hydrogen carrier due to its extremely high energy density (hydrogen density), ease of storage and transportation as a liquid, and carbon-free nature. Direct utilization of ammonia in high-temperature solid oxide fuel cells (SOFCs) has been demonstrated over the past decade. Concurrence of *in situ* endothermic ammonia decomposition and exothermic electrochemical hydrogen oxidation permit efficient heat integration. In this study, the experimental analyses of axial temperature and concentration profiles along the tubular SOFC (*t*-SOFC) fed directly with ammonia are performed to investigate the coupled ammonia decomposition and hydrogen oxidation reactions as well as the effect of polarization. Fast ammonia decomposition over the Ni catalyst is evident at the inlet of *t*-SOFC and complete ammonia conversion is confirmed above 600ºC. It is found that direct ammonia-fueled *t*-SOFC and an equivalent hydrogen-nitrogen fueled *t*-SOFC provide identical performances. With 100 SCCM of ammonia fuel feed, a maximum power of 12.2 W and fuel utilization of 81% are obtained at 800ºC in a *t*-SOFC with active area of 32 cm^2. The temperature and concentration profiles validate that the efficient heat integration inside ammonia-fueled *t*-SOFC is feasible if *t*-SOFC is operated at the temperature of 700ºC and below. The 23-hour performance test and SEM-EDS images of the fresh and used Ni-YSZ cermet surfaces confirm uniform performance and good durability of ammonia *t*-SOFC.

Acknowledgements

I am grateful for the support and encouragement given to me from my family and friends for the last two years. I would like to thank Prof. Teixeira, Prof. Datta, and Joshua Persky for their guidance and supports on this research. Special thanks to my labmates both in Teixeira Lab and Timko Lab for their helps and cheerful discussion and laughter. I also want to acknowledge Alex Molnar, Nick Sounthala, and Paul Osenar from UpStart Power, Inc. for providing the equipment for this research.

Thank you all.

Table of Contents

List of Figures

List of Tables

Chapter 1

Introduction and Background

1.1 Hydrogen economy and ammonia as a hydrogen carrier

The warming influence of greenhouse gases in the atmosphere has increased substantially over the last several decades. Annual greenhouse gas index (AGGI), which was reported in U.S. Global Change Research Program [1], increases over 40% since 1990. Carbon dioxide remains the largest contributor among the greenhouse gases. On the global scale, greenhouse gas emissions result from several human activities, with fossil fuel consumption as the main contributor.

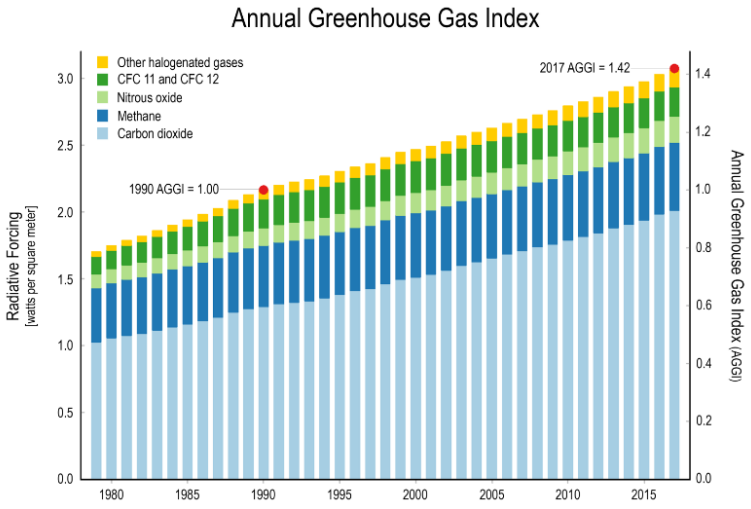

Figure 1: Annual greenhouse gas index (AGGI) is 1.42 in 2017 and has increased by 40% since 1990. Carbon dioxide (light blue) represents over 60% of greenhouse gas emissions [1].

With rising concerns about pollutions, climate changes, availability and drawbacks of fossil fuels, hydrogen economy is proposed as being an attractive part of the future low-carbon economy. Hydrogen is considered as the clean fuel as its combustion only produces water. Numerous researches committed to investigate the development of hydrogen economy continue to grow over the past few decades. Figure 2 shows the clean concept of hydrogen economy where hydrogen can be produced by electrolysis of water, and reforming or pyrolysis of biomass [2]. However, these process could not generate sufficient amount of energy to satisfy the domestic or global energy needs or requirements.

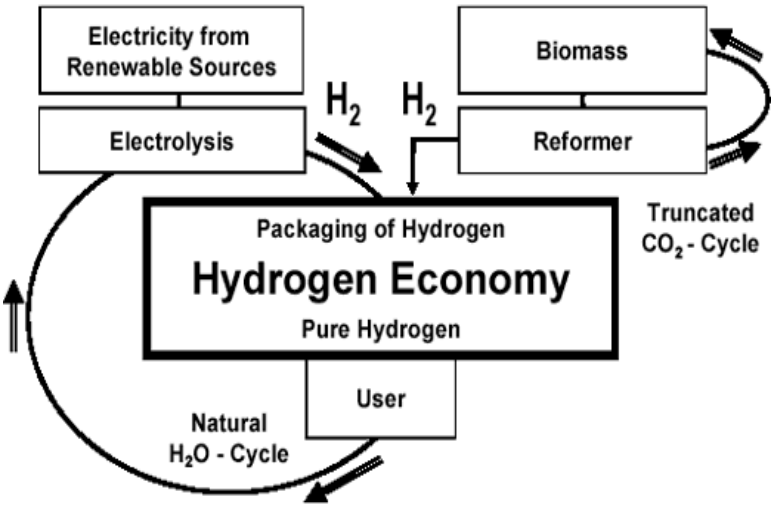

Figure 2: A clean concept of hydrogen economy which hydrogen is produced for the consumers by: (1) electrolysis of water and (2) reforming or pyrolysis of biomass [2].

Despite considerable advantages of hydrogen economy over hydrocarbon economy, there are several limitations and challenges associated with the

infrastructure for storing and transporting hydrogen gas due to its light nature. So, it has been of interest to investigate the use a suitable hydrogen carrier instead [3].

Ammonia could be a promising hydrogen carrier in many aspects: (1) it is produced at essentially the same cost as hydrogen, (2) it is available in large quantities than any other pure chemicals, and (3) it is distributed through an existing, world-wide infrastructure. Ammonia fuel cycle is shown in Figure 3 [4], the cycle involves the reduction of nitrogen coupled with oxidation of water, followed by ammonia decomposition into nitrogen and hydrogen gases, and then the produced hydrogen can be used to generate electricity via electrochemical reaction. In this sense, ammonia offers the solutions to both hydrocarbon economy and hydrogen economy related challenges [3,5].

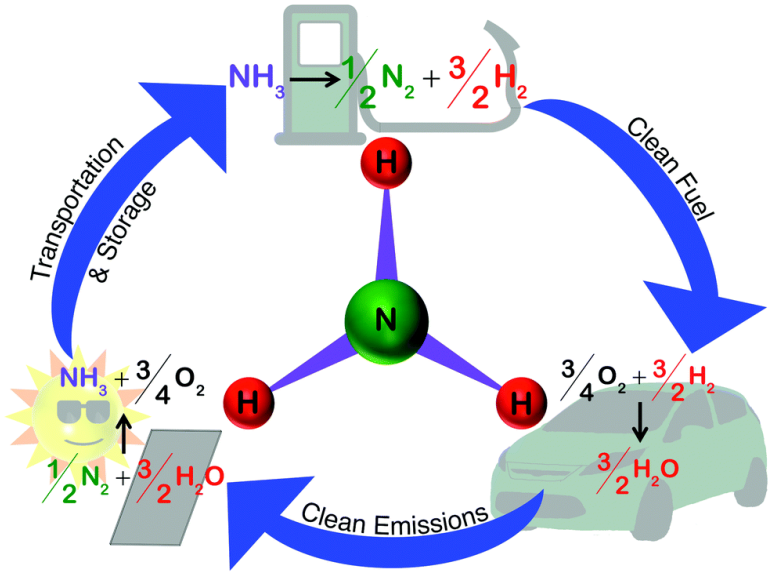

Figure 3: The sustainable ammonia fuel cycle [4].

1.2 The tubular solid-oxide fuels (*t*-SOFCs)

With the ability to efficiently provide electrical power while generating very much lower pollutant emissions, fuel cell technology serves as a promising alternative to the conventional heat engine. There are various types of fuel cells which are typically classified on the basis of the electrolyte used. Types of electrolyte dictate a range of operating temperature, fuel chemistry at the electrodes, and catalyst for fuel cell system [6,7].

A fuel cell is a device that directly converts the chemical energy from a fuel into electrical energy through electrochemical reactions. Fuel cell has four main parts: anode, cathode, electrolyte, and an external circuit. The chemical energy of a fuel, or reductant, is released via its reaction with an oxidant, usually oxygen, fed to the anode and cathode, respectively. The energy is collected as electricity by the external circuit. The circuit is completed by the transport of an anion or a cation through the electrolyte. Among different types of fuel cells, the solid-oxide fuel cell (SOFC) is the only true solid electrolyte fuel cell and has the highest range of operating temperatures: from 500ºC to 1,000 ºC [8]. The two most common geometries of SOFC are planar and tubular cells. The materials for cell components in these different geometries are either the same or very similar, just different in shape [9]. However, the tubular SOFC (*t*-SOFC) is typically more robust in terms of its ability to handle thermal and mechanical stresses, while providing better sealing and active area as compared to the planar cell [10,11].

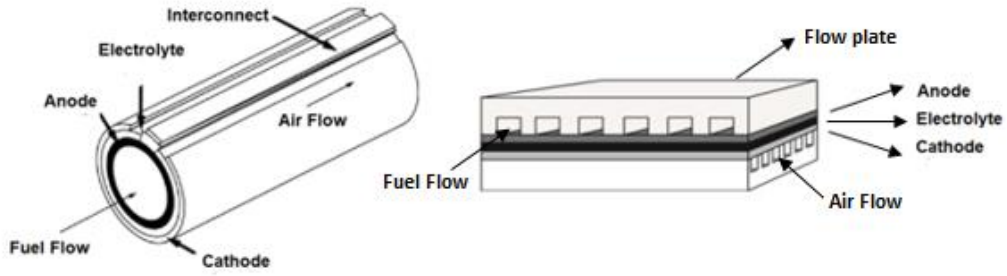

Figure 4: Tubular (left) and planar (right) solid oxide fuel cell configurations [12]

The conventional SOFC operates at atmospheric pressure and an elevated temperature form 700ºC to 1,000ºC. A high-temperature SOFC has several advantages over other low-temperature fuel cells: (1) fast electrochemical reaction rates are possible with low cost catalyst such as nickel; (2) low ohmic loss and high ionic conductivity in the ceramic electrolyte; (3) high tolerance to contaminant; (4) fuel flexibility; (5) and high quality waste heat that can be recovered [6,13]. A number of different fuels can be directly utilized without the pretreatment process or external reformer because internal reforming or cracking reactions are favorable at the elevated temperatures. These conventional fuels are mostly hydrocarbons such as syngas, biogas, bio-ethanol, bio-methanol, etc [14]. However, with hydrocarbon fuels, the carbon deposition on traditional nickel anode becomes serious issue [11]. Severe coking reduces cell performance and leads to premature cell degradation. Other challenges associated with SOFC are sealing, thermal expansion mismatch, interconnect, and component issues [11,13].

Substantial research efforts have been invested over the past few decades to address existing performance issues and to make SOFC systems commercially viable. The two main areas of investigation are the development of new SOFC components to avoid coking and the exploration of suitable alternative fuels for commercial SOFCs [15]. In fact, the selection of a fuel substitute which does not contain carbon atom is one such promising strategy to avoid coking and rapid degradation of cell performance.

1.3 Ammonia as an attractive fuel for SOFCs

Hydrogen is known to be an ideal fuel for fuel cells. Hydrogen-powered fuel cells are not only pollution-free but also far more efficient than traditional combustion technologies. However, hydrogen is not economical to store and transport. It is light and volatile and has a low flash point thus presenting a safety issue [16]. Selection of a practical alternative fuel or hydrogen carrier is an important step to commercialization of SOFCs.

A proper fuel should be economically viable, readily available, and safe to store and transport [17]. Many research groups have investigated the feasibility of a direct utilization of different hydrocarbons for SOFCs whereby the fuel is reformed into hydrogen within the cell. The major problem facing this technology is severe coking over the nickel anode. In this sense, ammonia is a good substitute fuel for both hydrogen and hydrocarbons because it is relatively cheap, easy to store and transport, carbon-free, less flammable than other fuel [18,19]. Ammonia can also be easily liquefied and the volumetric energy density of liquefied ammonia is higher

than that of liquid hydrogen [15]. Even though the toxicity of ammonia can be a concern, this challenge have largely been resolved by the successful designs of ammonia handling and storage systems. Due to the aforementioned features, ammonia serves as a promising feedstock to make SOFCs more commercially viable and reliable [16].

1.4 Ammonia-fueled SOFCs

Many research groups have investigated the feasibility and efficiency of ammonia-fueled SOFCs. Wojcik et al. and Staniforth and Ormerod were the first to demonstrate that direct usage of ammonia in SOFCs is feasible. In fact, they claim it could work very well even with conventional SOFCs containing nickel anodes because nickel is also a good catalyst for ammonia cracking reaction [20,21]. These hypotheses were experimentally supported a few years later with additional explanation on how the ammonia-fueled SOFCs system works. Internal ammonia cracking reaction into nitrogen and hydrogen gases in SOFCs is promoted at an elevated operating temperature [15,22,23]. Possible overall reactions include:

Anode:
$$4NH_3 + 6O^{2-} \rightleftharpoons 2N_2 + 6H_2O + 12e^- \quad (1)$$

$$2NH_3 + 5O^{2-} \rightleftharpoons 2NO + 3H_2O + 10e^- \quad (2)$$

$$2NH_3 \rightleftharpoons N_2 + 3H_2 \quad (3)$$

$$H_2 + O^{2-} \rightleftharpoons H_2O + 2e^- \quad (4)$$

Cathode:
$$O_2 + 4\,e^- \rightleftharpoons 2O^{2-} \quad (5)$$

The direct electrochemical oxidation of ammonia (1, 2) does not occur in SOFC. Instead, the reactions proceed in a two-stage process: in which (3) ammonia gas is first decomposed into nitrogen and hydrogen gases over the nickel cermet anode, then (4-5) hydrogen is oxidized electrochemically with oxygen anions diffusing from the cathode via the electrolyte to generate power [15,19].

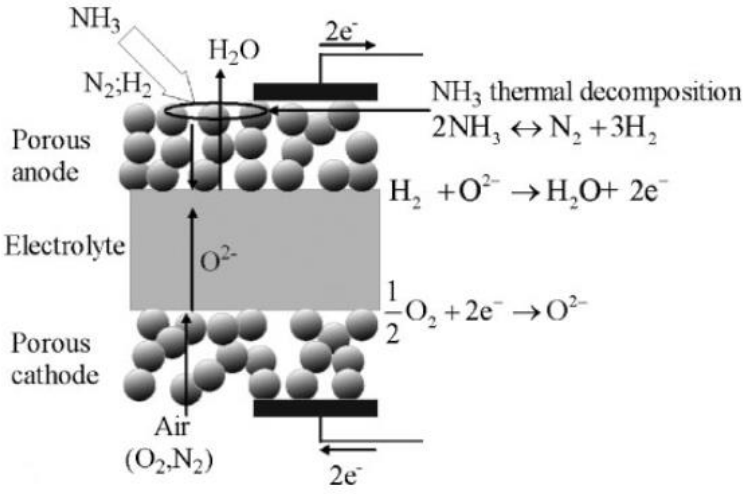

Figure 5: Working principles of oxygen ion-conducting SOFC fed with ammonia gas [24].

The two-stage process of ammonia-fueled SOFCs has been confirmed by other research groups [23,25,26]. Hydrogen is the only gas to react electrochemically in the system, while nitrogen is an inert. This is why the performance of ammonia-fueled SOFCs is similar to that of an equivalent hydrogen-fueled SOFC. However, the complete conversion of ammonia into hydrogen and nitrogen is desired in order to achieve high performance and good durability of SOFCs. Sufficient conversion, above 90%, of ammonia in fact can be obtained at elevated temperatures above 700ºC [15,22,27].

One of the concerns associated with the direct usage of ammonia in SOFCs was the potential undesired formation of nitrogen oxides (NOx) gas. It is theoretically stated that oxidation of nitrogen into NOx is possible and increases with temperature [24,28]. But it was later reported experimentally that the actual amount of produced NOx is very small and negligible [23,24,25–28]. The presence of ammonia could also possibly suppress NO formation, as it is used in the selective catalytic reduction of nitrogen oxides [29,30].

The performance and power output of ammonia-fueled SOFCs have thus been substantially investigated and proven to be almost identical to that of an equivalent hydrogen-fueled SOFCs, making ammonia a very promising carrier of hydrogen as compared with conventional hydrocarbon fuels [24,25,28,31,32]. Hydrogen-fueled SOFCs usually show slightly better results because there is a higher partial pressure of hydrogen in the anode channel. When ammonia is used an internal cracking reaction is expected, the co-produced nitrogen causes dilution of hydrogen [15,22]. Despite its preliminary successes, the major challenge in realizing this process remains with the intensification of the cell design, particularly with coupling of the exothermic/ endothermic reactions and high reaction rates.

1.5 Coupling of endothermic and exothermic reactions

Ammonia-fueled SOFCs also give other notable advantages over hydrogen-fueled SOFCs. These advantages are due to the internal endothermic ammonia cracking. For both cases, the only electrochemical reaction in the anode is known to be an exothermic hydrogen oxidation reaction (HOR) with standard enthalpy of -

241.8$\frac{\text{kJ}}{\text{mol H}_2}$. When ammonia is used as a fuel, an endothermic cracking reaction with a standard enthalpy of +46.1 $\frac{\text{kJ}}{\text{mol NH}_3}$ or +30.7$\frac{\text{kJ}}{\text{mol H}_2}$ consumes 13% of the heat generated from the HOR, thus increasing the efficiency of the system [15,23,31].

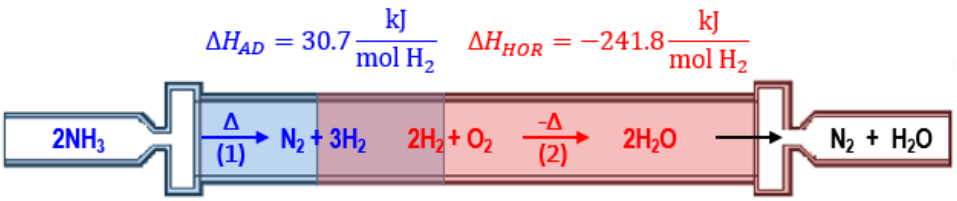

Figure 6: The two-stage process of ammonia t-SOFCs. Ammonia is first endothermically decomposed ($\Delta \text{H}_{\text{AD}} = 30.7\ \text{kJ/mol H}_2$). Then, the produced hydrogen is oxidized ($\Delta \text{H}_{\text{HOR}} = -241.8\,\text{kJ/mol H}_2$) to generate electricity. There is a partial overlap of the ammonia decomposition and the HOR regions.

The positive influence of this cooling effect on the temperature field, gas transport and power output of SOFCs was first investigated by Meng Ni in 2011 [32]. Modeling simulations were used to understand how ammonia thermal cracking affects the SOFC performance. The temperature field of the SOFC is determined by: (1) rate of the endothermic ammonia cracking; (2) enthalpy change of the electrochemical reaction; and (3) overpotential losses in the SOFC. It is reported that, for an ammonia-fueled SOFCs, temperature decreases along the SOFC. Moreover, the temperature gradient along the SOFCs is enhanced at higher operating temperatures because thermal cracking rate is exponentially dependent on temperature. In short, faster cracking reaction rate at an elevated temperature leads to a larger temperature gradient in the SOFC. This phenomenon complicates

the understanding of gas transport, coupled reaction processes, and electrical performance of SOFCs.

Experimental temperature measurement in ammonia-fueled SOFCs were carried out by Cinti et al [25,31]. The group used the commercial planar fuel cells to perform the comparative study and investigate the cooling effect and its benefits. Their final aim was to achieve thermal equilibrium and higher electrical efficiency. It was found that the temperature of ammonia-fueled SOFCs was always lower than that of an equivalent hydrogen-nitrogen mixture indicating the heat integration. The use of ammonia also permits a better control of SOFCs temperature field and a smaller air flow rate because less external cooling is needed to dissipate the heat produced.

Long-term stability of ammonia-fueled SOFCs has also been investigated by Yang et al [27]. As mentioned earlier, the complete decomposition of ammonia is desired and is possible at temperatures above 700ºC. Presence of ammonia at low temperature region can lead to premature degradation of SOFCs. If ammonia is not fully cracked, the nickel surface of anode might be nitrided resulting in volumetric change, increase in ohmic overportential, and cell delamination. Therefore, a careful design of cell and operating conditions is required to avoid such degradation phenomenon. Tubular cells could ensure more complete conversion of ammonia by providing more residence time and operation more like a plug flow reactor (PFR) than a planar cell that behaves more like a continuous stirred-tank reactor (CSTR).

1.6 Objectives

The usage of ammonia as an alternative fuel to hydrogen and hydrocarbons fuels in SOFCs has thus been validated theoretically and experimentally in the literature. The benefit of cooling effect from a coupled endothermic ammonia decomposition has received attention for potentially achieving superior control of thermal gradients in SOFCs. Currently, comprehensive study and experimental analyses of cooling effect on ammonia-fueled SOFCs are limited, however, the intensified, integrated process has not been well-studied in an integral cell.

In this work, we make substantive strides toward realizing the sustained, autothermal operation of direct ammonia *t*-SOFCs which the internal ammonia decomposition proceeds without external input of energy. The *t*-SOFCs achieves realistic reaction environments that allow for the systematic and thorough evaluation of temperature and concentration profiles as the measurements can be resolved axially along the anode channel of *t*-SOFC. We hypothesize that performance and stability can be optimized by revealing and characterizing thermal and concentration gradients within the reactor. Extent of endothermic ammonia decomposition reaction and operating conditions for maximum power output and fuel utilization are evaluated.

Chapter 2

Materials and Methodology

2.1 Experiment setup

A custom built fuel cell test stand was designed and assembled as described in the schematic diagram of the experimental setup shown in Figure 7.

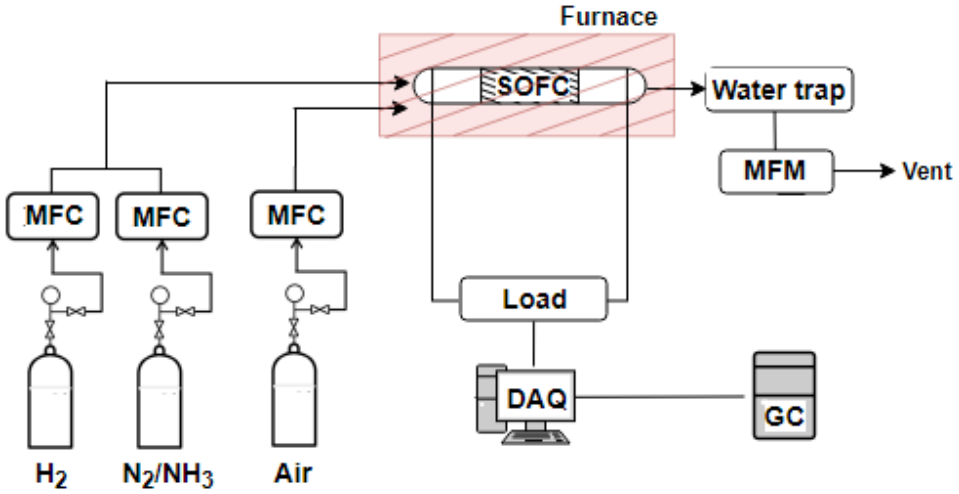

Figure 7: Process flow diagram for *t*-SOFC experimental setup. H_2, N_2, and/or NH_3 were fed through MFCs to the inner anode tube, while air passed to the outer cathode. An electronic load with data acquisition monitored power generation, and in-line GC was used to monitor conversion.

The *t*-SOFC was placed within a 30-cm tubular furnace which is insulated at either end with ceramic plugs. The fuel cell was connected to the electronic load bank with a data acquisition system which was used to monitor the output of *t*-SOFCs. Various gas cylinders were connected to the fuel cell's inlet via mass flow

controllers (MFCs). A gas chromatography (GC) and a mass flow meter (MFM) were connected to the outlet for anode effluent gas analysis.

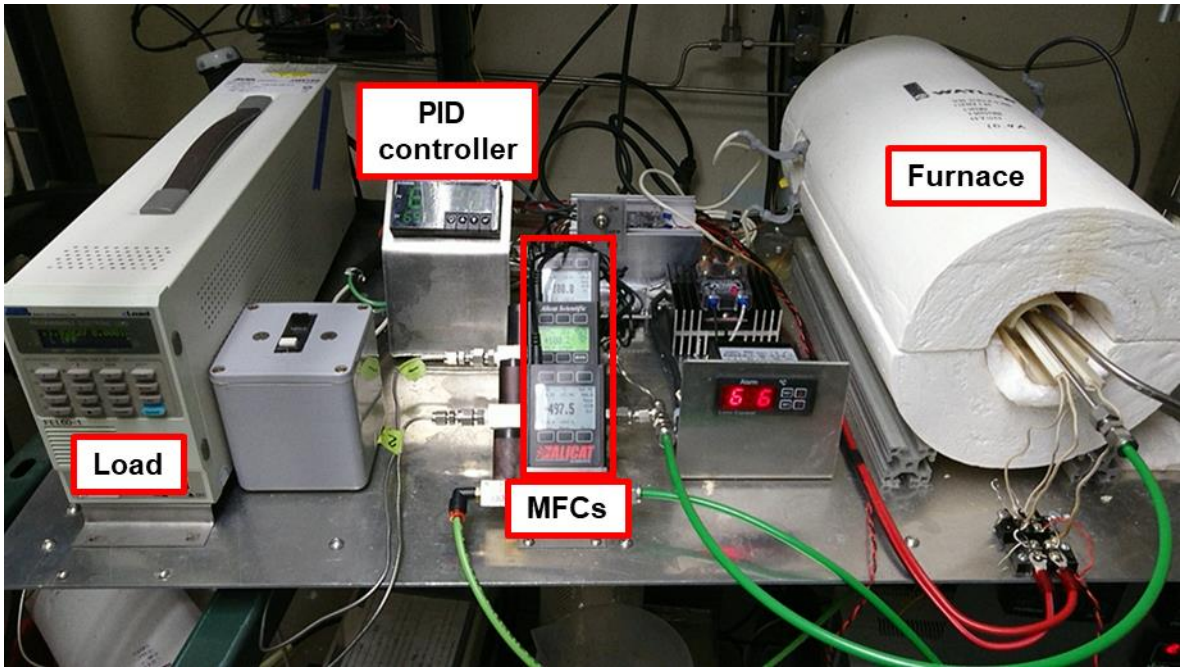

Figure 8: Test stand included major components of experimental setup. The *t*-SOFC was placed on the ceramic shell within the tubular furnace which was equipped with PID controller and K-type thermocouple located at the center. The furnace was insulated with ceramic plugs and ceramic fiber insulation

The gas flow controllers for air, hydrogen, nitrogen and ammonia were Alicat Scientific mass flow controllers with model numbers MC-500SCCM-D, MC-500SCCM-D and MCS-500SCCM-D respectively. The Watlow 120V 1250W ceramic fiber furnace (model number VS405A12S-0001R) was equipped with Omega PID controller (model number CN8DPT-225-006) and K-type Omega thermocouple (model number KMQIN-062U-24) located at the center. The *t*-SOFC was connected to an American Reliance, Inc. (AMREL) load bank (model number

FEL 60-1). Transient current and voltage data were controlled and logged in data acquisition software (LabVIEW) developed at WPI. An effluent gas from a *t*-SOFC was analyzed by an in-line micro-GC (490 Micro GC; Column 1: Molsieve 5A with He carrier gas, Column 2: PoraPLOT Q with Ar carrier gas) from Agilent Technologies and mass flow meter (model number M10MB52CS3BV-S) from MKS Instruments, Inc.

2.2 Temperature gradients in the furnace and *t*-SOFC placement

The tubular furnace was not truly isothermal and had significant amount of heat loss at both ends. Temperature profile within the furnace was evaluated in order to select the optimal placement for *t*-SOFC. Temperature profile within the furnace at operating temperature of 900ºC is shown in Figure 9. It is found that the optimal placement, which uniform temperature was maintained close to 900ºC, for *t*-SOFC was located at 9cm to 19cm from the inlet. Temperature profiles at different conditions are available in Appendix A.2.

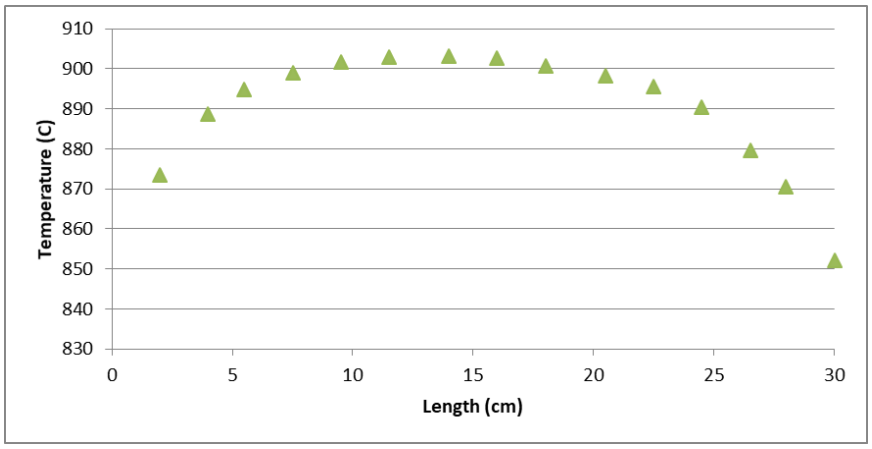

Figure 9: Temperature profile within a furnace operated at 900ºC. The optimal location, which uniform temperature was maintained, for *t*-SOFC is from 9cm to 19cm.

2.3 *t*-SOFC and cell preparation

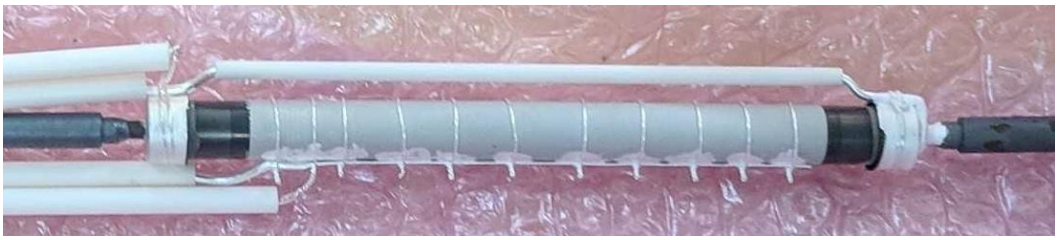

Figure 10: The t-SOFC fabricated by Upstart Power, Inc.

The tubular cells used in this study were fabricated at Upstart Power, Inc. and identical to those used in previous studies [11]. Each cell had an active area of 32 square centimeter, a length of 100 millimeter, and a diameter of 10.2 millimeter. This anode-supported cell (ASC) had a nickel-yttria stabilized zirconia (Ni-YSZ) anode, with a thickness of 1 millimeter; a YSZ electrolyte (oxygen ion-conducting) with a thickness of 15 micrometer; and a lanthanum strontium cobalt ferrite (LSCF) cathode with a thickness of 30-50 micrometer.

Table 1: *t*-SOFC Specification

Fuel cell specifications			
Anode	Ni -YSZ	1000	µm
Electrolyte	YSZ	15	µm
Cathode	LSCF	30-50	µm
Active area		32	cm^2
Length		100	mm
Diameter		10.2	mm
Shape	Circular tube		

To prepare the fuel cell, a *t*-SOFC was placed in the tubular furnace and was heated to 900 ºC in the presence of pure hydrogen for three hours to reduce any

nickel (II) oxide into a metallic nickel. The cell was then operated at constant current density for one hour before any polarization data or gradients analyses were obtained. The shut-down procedure involved cooling the cell with presence of hydrogen gas to avoid premature delamination.

2.4 Experiment: temperature and concentration gradients

An expanded diagram of *t*-SOFC setup for axial temperature and concentration profiles analyses was shown in Figure 11.

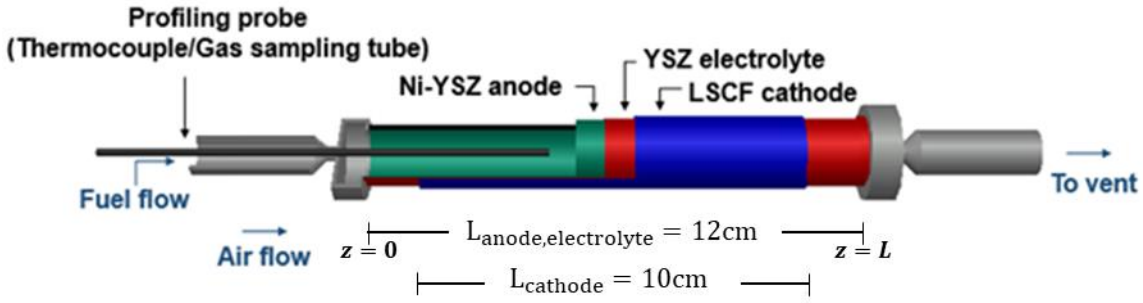

Figure 11: Expanded diagram of *t*-SOFC showing the internal fuel path (anode), external oxidizer path (cathode), and corresponding wall-coated catalyst. Temperature and concentration profiling was achieved by linear actuation (z-direction) of thermocouple or tubing probe.

The 1/16” K-type Omega thermocouple with model number KMQIN-062U-24 was used for axial temperature profile analyses. As for the analyses of concentration profile, a 1/16” stainless steel tube (60 cm) and the 10 mL gastight syringe (Hamilton 1010 LTN SYR) were used.

To perform the temperature profile analyses of *t*-SOFC with different fuel gases, a thermocouple was manually slid along the *t*-SOFC from the downstream side during operation at various constant current densities and furnace

temperatures. Temperature gradients along the *t*-SOFC were averaged over 120 seconds and recorded to account for any variation due to the on-off control employed by the furnace. A list of operating parameters for temperature gradient analyses is summarized in Table 2.

Table 2: *t*-SOFC operating parameters for temperature profiles experiments

Operating parameters			
Fuel 1	H_2	150	SCCM
Fuel 2	H_2:N_2	150:50	SCCM
Fuel 3	NH_3	100	SCCM
Air		500	SCCM
Temperature		700, 800, 900	ºC
Current		0, 5, 10, 15	Amp

Three anode fuel gas flow rates including 150 SCCM hydrogen gas, gas mixture of 150 SCCM hydrogen and 50 SCCM nitrogen, and 100 SCCM ammonia gas were utilized. On a molar basis, the equivalent hydrogen flowrates were held constant to achieve the same molar hydrogen feed rate. The air flow rate on the cathode side was maintained at 500 SCCM for all experiments, which is 1.4 times stoichiometric demand. Since high ammonia decomposition had been confirmed at temperature above 700ºC [15,22,27], testing temperatures of 700ºC, 800ºC, and 900ºC were initially chosen. Minimum operating voltage of 0.6 V was maintained due to limitation from the manufacturer to avoid degradation of the cell. After the polarization curves of each fuel at various temperatures were obtained, sets of axial temperature gradients along the *t*-SOFC were collected at 0A, 5A, 10A, and 15A.

To perform the concentration profile analyses, a gastight syringe was used to withdraw 10 mL of gas at 10 mL/min from anode channel through a 60-cm 1/16" stainless steel tube, which was placed inside *t*-SOFC. Then the manual injection to micro-GC was performed. A tubing probe was then manually slid along the *t*-SOFC from the downstream side for the next measurement site. A list of operating parameters for concentration profile analyses is summarized in Table 3.

Table 3: *t*-SOFC operating parameters for concentration profile experiments

Operating parameters			
Fuel 1	NH_3	100	SCCM
Air		500	SCCM
Temperature		550,600,650,700	ºC
Current		0, 5, 10	Amp

In order to observe the effect of temperature on the extent of ammonia decomposition reaction, a set of experiments using ammonia gas was performed at open-circuit voltage (OCV) and testing at the lower temperatures of 500ºC, 600ºC, 650ºC, and 700ºC. Additionally, concentration gradients inside an operating *t*-SOFC at 5A and 10A were measured at a furnace temperature of 700 ºC to observe the effect of operating current on the concentration profile.

Chapter 3

Results and Discussion:

Performance, Temperature and Concentration Profiles

Complete experimental results are available in the Appendix A.

The overall experimental study is systematically divided:

(1) to establish the operating parameters of the direct ammonia-fueled *t*-SOFC for maximum power output,

(2) to compare the performance between the ammonia-fueled *t*-SOFC and an equivalent hydrogen-fueled *t*-SOFC, and

(3) to evaluate the extent of endothermic ammonia cracking and its beneficial heat integration via axial temperature and concentration profiles.

3.1 Identical performance to pure hydrogen *t*-SOFC

The performance of a fuel cell is governed by its polarization curve which shows the electrochemical efficiency of the fuel cell at any operating current. Fuel cells achieve the highest voltage output at open circuit or ‘zero current’ condition. The voltage drops off as the withdrawn current increases. There are three major causes to voltage losses with increasing current: the activation loss, ohmic loss, and concentration loss [33]. Activation loss is caused by the voltage overpotential required to overcome the activation energy of electrochemical reaction on the catalytic surface of electrodes. Activation polarization typically dominates loss at low current density. Ohmic loss corresponds to the voltage loss due to the intrinsic electrical resistance to charge transport in the cell component, i.e. the electrolyte. The concentration loss results from the diffusional limitation or the concentration of reactants at the catalytic surfaces of electrodes and typically dominates losses at high current density.

A total of nine polarization curves, representing three compositions at three different temperatures, are recorded and plotted together with their nine corresponding curves for power outputs as shown in Figure 12. The results from all of the three gases lead to the following observations: (1) higher OCV and higher activation polarization are observed at lower temperatures and lower current density, (2) at the moderate current densities, highest voltages are obtained at 800 ^{o}C and highest ohmic loss (steep slope) is observed at 700^{o}C, (3) at high current densities, i.e. above 20A, higher voltage could be obtained at higher temperatures

which diffusional limitation is less expected, and (4) maximum power output is achieved at 800 ºC.

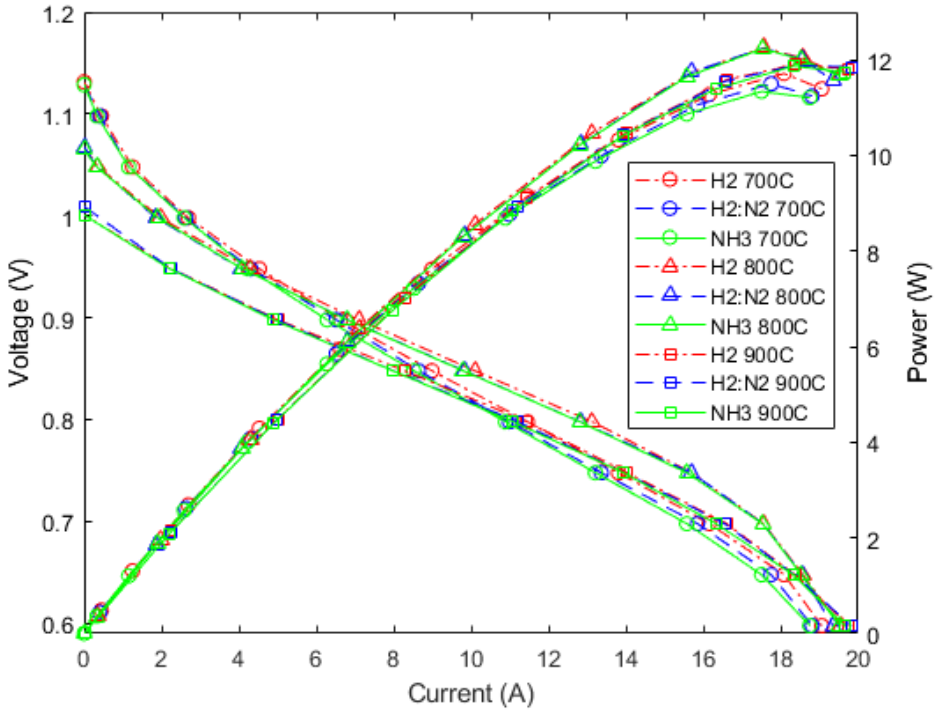

Figure 12: Polarization curves of three fuels of equivalent hydrogen molar flowrate; 150SCCM H_2 (dash-dotted line), 150:50SCCM H_2 and N_2 (dash line), and 100SCCM NH_3 (solid line), at 700ºC (o), 800ºC (Δ), and 900ºC (□). Ammonia and hydrogen *t*-SOFCs provide identical electrical powers. Higher OCV is observed at lower temperature. Maximum power output of 12.2 W is achieved at 800ºC.

It is worth noting here that the observed ohmic losses due to charge transport at 800ºC and 900ºC are similar and almost identical. This can be a reason why maximum power is observed at 800ºC not 900ºC. The numerical data at different temperatures for conditions of maximum power are given in Table 4.

Table 4: Operating parameters at maximum power outputs

Temperature (°C)	Fuel Feed	Voltage (V)	Current (A)	Power (W)	Fuel Utilization (U_f)	FC Efficiency (ε)
700	H_2	0.65	18.1	11.7	0.84	0.43
	$3H_2$:$1N_2$	0.65	17.8	11.5	0.83	0.43
	NH_3	0.65	17.5	11.3	0.81	0.48
800	H_2	0.70	17.6	12.3	0.82	0.46
	$3H_2$:$1N_2$	0.70	17.5	12.2	0.81	0.45
	NH_3	0.70	17.5	12.2	0.81	0.52
900	H_2	0.65	18.4	11.9	0.85	0.44
	$3H_2$:$1N_2$	0.65	18.3	11.9	0.85	0.44
	NH_3	0.65	18.3	11.9	0.85	0.50

The fuel utilizations (U_f) were calculated as a ratio of the actual current, *I*, to the maximum current I_{max} that would result if all of the fuel were consumed[11], where I_{max} =$2\mathrm{Fn}_{\mathrm{H}_2,0}$. *F* is Faraday's constant; 2 is the number of electrons per hydrogen molecule; and $n_{H_2,0}$ is the equivalent hydrogen molar feed flow rate.

$$U_f = \frac{I}{2Fn_{H_2,0}}$$

Fuel cell efficiencies were generally measured to be between 40-60%, indicating that about half of the potential chemical energy of the feed was converted to useful electrical power, while the remaining energy was excess thermal heat. The fuel cell efficiencies (ε) were calculated as a ratio of the electric work per mol of hydrogen, W_E, to the overall enthalpy change of reactions, ΔH_{OR}. $W_E = P/\ n_{H_2,0}$, where *P* is power.

$$\varepsilon_{H_2} = \varepsilon_{3H_2:1N_2} = \frac{W_E}{-\Delta H_{HOR}}$$

$$\varepsilon_{NH_3} = \frac{W_E}{-(\Delta H_{HOR} + \Delta H_{AD})}$$

As mentioned previously, the coupled endothermic ammonia decomposition reaction consumes 13% of the heat generated from the exothermic hydrogen oxidation reaction. This heat integration can increase the fuel cell efficiency around 5-7% under the specified experimental conditions.

Direct use of ammonia gas as a substitute for hydrogen gas is feasible as shown by the parity plot in Figure 13. At the same operating parameters, ammonia-fueled *t*-SOFC gives identical performance and better efficiency to those obtained from the equivalent hydrogen-fueled *t*-SOFC as shown in Table 4.

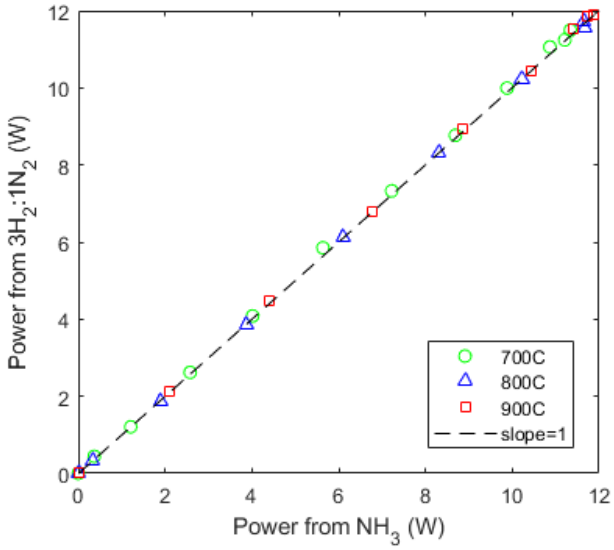

Figure 13: Parity plot comparing electrical powers of the ammonia fuel (x-axis) and the equivalent hydrogen fuel (y-axis) taken at the same voltages. The line fitting of all data points shows the slope of one demonstrating that the two fuels operate nearly identical performance.

Pure hydrogen fuel gives slightly higher current densities due to its higher partial pressure of hydrogen gas in the anode channel, as stated by Fuerte et al. and Ma et al. [15,22]. In fact, this effect is less significant as the operating temperature increase above 700 ºC because diffusivity of oxygen ions is greatly enhanced at elevated temperatures, thus, favoring the electrochemical hydrogen oxidation rate even under lean conditions. Since the performance of an ammonia-fueled *t*-SOFC is identical to an equivalent hydrogen-fueled fuel cells, it is evident that the reactions inside the anode channel proceed in essentially a sequential two-stage process. In other words, hydrogen oxidation is the only electrochemical reaction in the fuel cell. However, it should be noted that complete conversion of ammonia into hydrogen and nitrogen gases is desired in order to achieve identical performance to that of hydrogen-fueled fuel cell.

3.2 Revealing temperature gradients in direct ammonia *t*-SOFCs

A thermocouple placed inside the anode channel of *t*-SOFC was manually slid along the length of the *t*-SOFC from the downstream side. Transient temperature data were recorded and averaged. It should be noted that the reactive or catalyzed zone of *t*-SOFC for ammonia decomposition $(\mathrm{L}_{\mathrm{anode,electrolyte}} = 12\mathrm{cm})$ is located from -1 cm to 11 cm and the catalyzed zone for the electrochemical hydrogen oxidation $(\mathrm{L}_{\mathrm{cathode}} = 10\mathrm{cm})$ is located from 0 cm to 10 cm. The temperature profiles of three fuel gases at various furnace temperatures and operating currents are summarized in Figures 14-17.

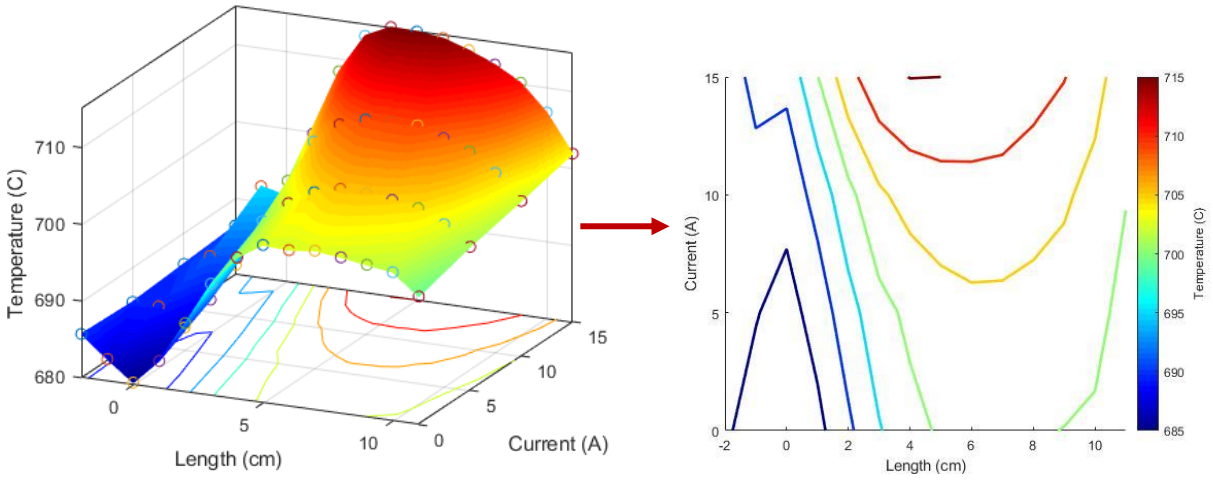

Figure 14: 3D mesh diagram with the projected contour plot of temperature profiles of ammonia *t*-SOFC at different operating currents and a furnace temperature of 700ºC. Local temperatures are represented by color; from navy blue (cold) to dark red (hot).

The 3D mesh diagram with the projected contour plot of temperature profiles of ammonia *t*-SOFC at a furnace temperature of 700ºC are shown in Figure 14. The 3D diagram and contour plot describe the relationships between the axial length of *t*-SOFC, the operating current, and local temperature. The recorded temperature data, which is represented by circles, is used to create the 3D mesh describing the temperature profiles inside *t*-SOFC. The corresponding contour plot is projected under the mesh diagram and local temperature is represented by a range of color from navy blue (low temperature) to dark red (high temperature). Axial length of measurement and the current are represented by x and y coordinates respectively.

In Figure 15, for example, local temperature of ammonia gas (solid line) is approximated at 685 ºC while those of pure hydrogen gas (dotted line) and hydrogen-nitrogen gas mixture (dashed line) are around 700 ºC at 1 cm and 5A.

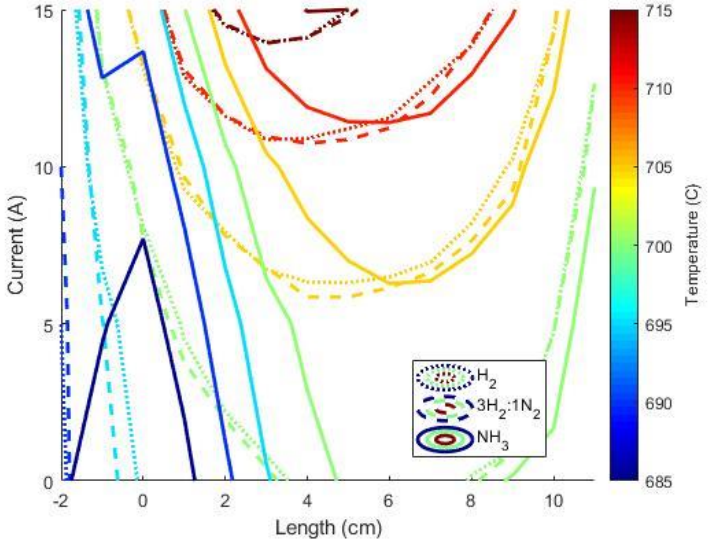

Figure 15: Contour plot of temperature profiles of three fuel gases at various operating currents and furnace temperature of 700 ºC. With ammonia fuel (solid line), the temperature inside the anode stays below 695ºC (blue) for 1cm from the inlet; while the temperatures of the hydrogen *t*-SOFCs range from 695ºC to 710ºC. Highest temperature drop of 15ºC is recorded at the inlet. Ammonia *t*-SOFC permits a shorter hot spot (dark red) at high current of 15A and allows better utilization of reactor. Ammonia decomposition in the first half of *t*-SOFC slow down the rate of hydrogen oxidation and balance the generated heat in the anode channel.

As clearly seen from Figure 15-17, the temperature gradients of ammonia gas feed are always lower than those of the pure hydrogen gas and hydrogen-nitrogen gas mixture. This indicates that an endothermic ammonia decomposition is occurring within the anode and does lower the local temperature around the inlet by few degrees Celsius. Temperature gradually rises along the length of the fuel cell as the exothermic hydrogen oxidation becomes more dominant and the ammonia gas is depleted. Larger temperature increases at higher operating currents over the

first half of the fuel cell are observed as the rate of hydrogen oxidation becomes more favorable.

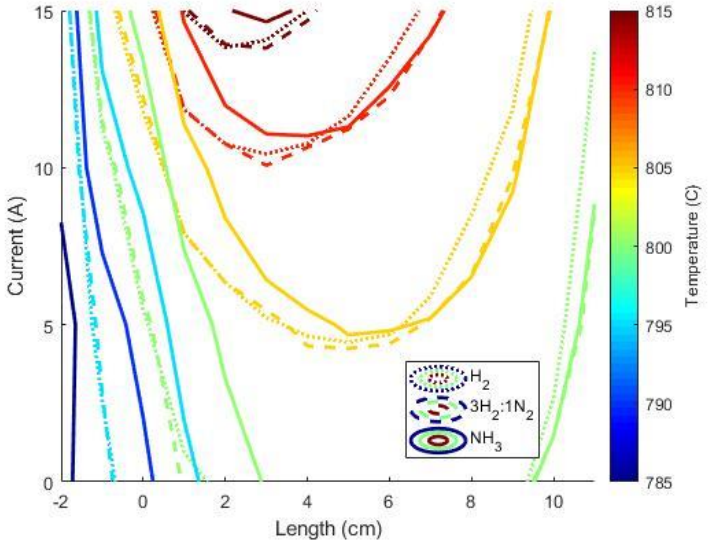

Figure 16: Contour plot of temperature profiles of three fuel gases at various operating currents and furnace temperature of 800 ºC. The forementioned cooling effect is reduced and larger hot spot is observed. The temperature drop at the cell inlet becomes less noticeable at 800ºC. Ammonia fuel's curves shift closer to the hydrogen's indicating lesser endothermic effect.

Temperature differences between ammonia fuel and the other two hydrogen fuels lessen as furnace temperature increases above 700 ºC. The cooling effect of ammonia decomposition is most noticeable at furnace temperature of 700 ºC, where temperature dips are observed at the beginning of catalyzed region (0 cm). At these furnace temperature and location, the rate of ammonia decomposition is more favorable than hydrogen oxidation which gives approximately the highest temperature drop of 15 ºC at OCV. Such phenomenon is not observed at 800 ºC and 900 ºC because the hydrogen oxidation is dominant at elevated operating

temperature and ammonia gas could possibly undergo thermal cracking prior to the inlet of the fuel cell.

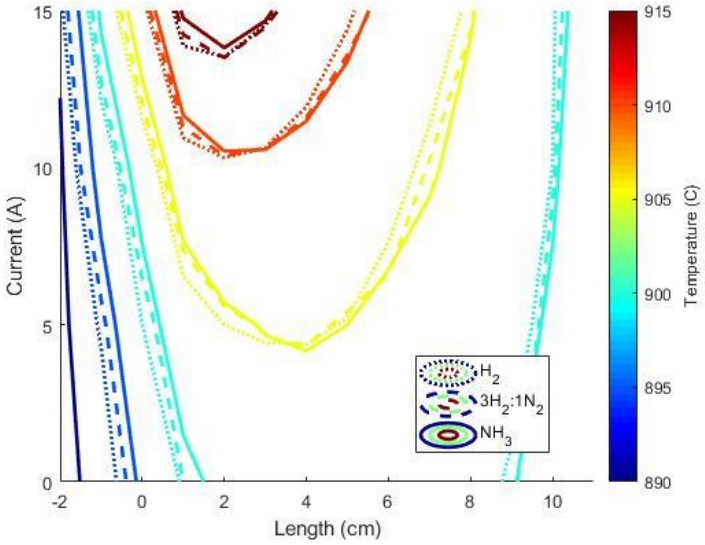

Figure 17: Contour plot of temperature profiles of three fuel gases at various operating currents and furnace temperature of 900 ºC. The overlaps of ammonia's curves with the equivalent hydrogen's describe identical thermal gradients within the anode. Ammonia is thermally cracked prior to the inlet and only hydrogen oxidation reaction occurs in *t*-SOFC.

The distinct influence of this endothermic ammonia decomposition reaction to temperature fields inside the anode channel of *t*-SOFC can be easily perceived by referencing the acquired temperature profiles to the furnace temperature profile, which is due to heat loss at the two ends of the tubular furnace. By doing so, temperature deviations (ΔT) resulting from endothermic decomposition reaction can be estimated as shown in Figure 18. Additional temperature profile analysis at a furnace temperature of 650 ºC was performed to confirm this trend of higher temperature drop around the inlet at lower furnace temperatures.

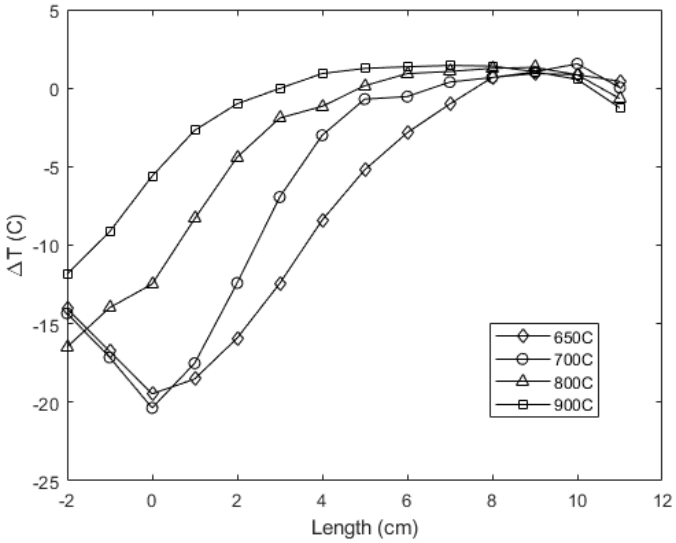

Figure 18: Temperature deviations at different furnace temperatures and OCV. These curves describe the thermal changes resulting solely from ammonia decomposition. Significant drops of temperature (valleys) are observed at 650ºC and 700ºC. Temperature deviations are smaller toward the end of *t*-SOFC as ammonia gas is depleted.

Comparing the trends at furnace temperatures of 650 ºC and 700 ºC, it is found that the temperature drop at the inlet is fairly equivalent but the axial temperature rise is slower at 650 ºC. The temperature profiles converge (ΔT=0) toward the end of *t*-SOFC indicating that complete ammonia conversion is achieved. As temperature increases from 650 ºC to 900 ºC, complete decomposition of ammonia is accomplished even sooner, approximately from 8 cm to 4 cm axial length.

3.3 Concentration profiles and the extent of endothermic ammonia decomposition

The concentration profiles were measured in the same manner as the temperature profiles as described previously. It should be noted again that the reactive or catalyzed zone of *t*-SOFC for ammonia decomposition ($\mathrm{L_{anode,electrolyte}} = 12\mathrm{cm}$) is located from -1 cm to 11 cm and the catalyzed zone for the electrochemical hydrogen oxidation ($\mathrm{L_{cathode}} = 10\mathrm{cm}$) is located from 0 cm to 10 cm. The 12-cm *t*-SOFC was located in the middle of 30-cm furnace. The fuel gases were fed via ¼" stainless steel tube. The concentration profiles and extent of endothermic ammonia decomposition in ammonia-fed *t*-SOFC at various furnace temperatures and operating currents are summarized in this section.

3.3.1 Concentration profile at OCV and different temperatures

To study only the extent of endothermic ammonia decomposition without any hydrogen oxidation, a set of concentration profiles were measured at OCV, i.e. at zero external current. Hydrogen oxidation does not theoretically occur at OCV and the dominant reaction is ammonia decomposition. Since a noticeable cooling effect is observed at the furnace temperatures below 700ºC from the temperature profiles, testing temperatures of 550ºC, 600ºC, 650ºC, and 700ºC were chosen. Ammonia concentration profiles at OCV and the various temperatures, and the corresponding plot for ammonia conversion in *t*-SOFC at OCV are shown in Figure 19. The conversion is calculated as one minus the concentration in the effluent divided by the concentration entering the anode.

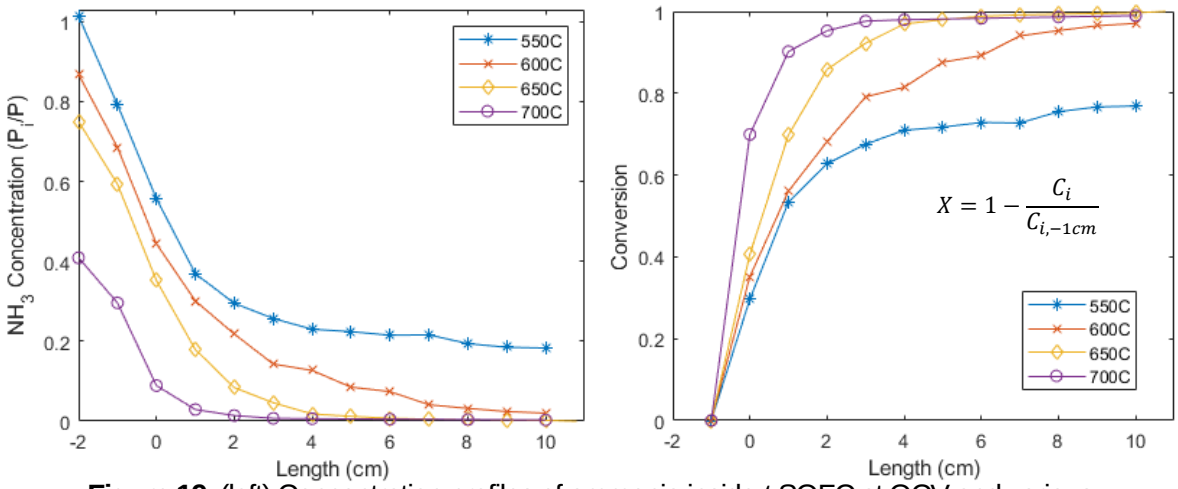

Figure 19: (left) Concentration profiles of ammonia inside *t*-SOFC at OCV and various temperatures, and (right) the corresponding ammonia conversion. Inlet ammonia concentration decreases with increasing furnace temperature, less than 50% of ammonia is remained at 700ºC. Results show that ammonia is thermally cracked prior to *t*-SOFC inlet at furnace temperature above 600ºC. Ammonia is not completely cracked at 550ºC.

The following observations may be made: (1) inlet concentration of ammonia decreases with increasing furnace temperatures, (2) ammonia is thermally cracked in the stainless steel tube prior to the cell inlet when the furnace temperature is more than or equal to 600 ºC, and (3) complete ammonia conversion is achieved within the tube at temperatures higher than 600 ºC.

Temperature deviation could be used as an indicator representing the degree of ammonia conversion. Figure 20 plots the ammonia concentration and temperature deviations at 650ºC and 700ºC. From the graph, both temperature curves gradually converge back to $\Delta T = 0$ as ammonia concentrations approach zero. The rate of ammonia consumption also corresponds to how fast the temperature curve converge back to zero. Complete conversion is expected when

the convergence is reached. Complete conversion of ammonia is approximately achieved at 8cm in *t*-SOFC for 650 ºC and 6cm for 700 ºC.

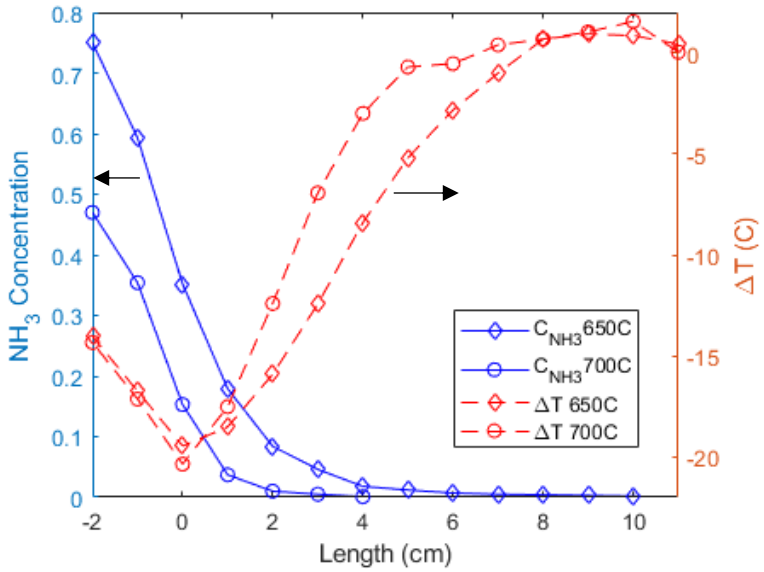

Figure 20: NH_3 concentrations profiles and the corresponding temperature deviations at furnace temperatures of 650 ºC and 700 ºC. Temperature deviation, or thermal change due to ammonia decomposition, correlates nicely with ammonia concentration within *t*-SOFC.

3.3.2 Estimation of ammonia decomposition's activation energy in *t*-SOFCs

The obtained concentration gradient at OCV is to be used to estimate the rate constant and activation energy of ammonia decomposition in Ni-YSZ anode channel of *t*-SOFCs. The t-SOFC acts as a plug flow reactor (PFR) and the axial length of the t-SOFC can be treated as the residence time the fuel feed spent in the reactor. The reaction is assumed to be first-order for simplicity.

First order rate law:

$$\frac{dC_A}{dt} = -kC_A$$

$$\ln\left(\frac{C_A}{C_{A0}}\right) = -kt$$

Arrhenius Equation:

$$\ln(k) = \ln(A) - \frac{Ea}{R}\left(\frac{1}{T}\right)$$

Ammonia concentrations along the *t*-SOFC is used to estimate the rate constant, k, and activation energy, Ea, as shown in Figure 21.

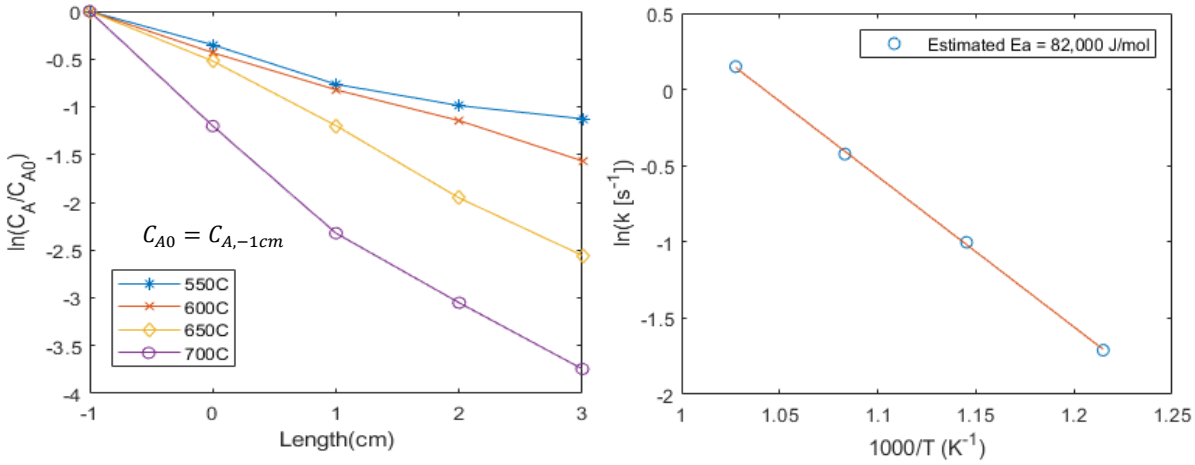

Figure 21: (left) Concentration profiles of ammonia at various temperatures and (right) Arrhenius plot describing the estimated rate of ammonia decomposition in *t*-SOFC. Apparent activation energy is 82,000 J/mol.

The activation energy is estimated to be 82,000 J/mol which is in agreement to the range of activation energies (71,000 to 92,000 J/mol) for ammonia decomposition in fuel cell application investigated by Choudhary et al [34].

3.3.3 Concentration profiles of *t*-SOFCs with current

Since the concentration profiles of ammonia-fueled *t*-SOFCs are governed by the overall reactions, the two-stage coupled reactions; the experimental observations under closed circuit conditions when a current is drawn with presence of exothermic hydrogen oxidation are also evaluated. The comparison of concentration profiles at 700 ºC and different operating currents are plotted in Figure 22.

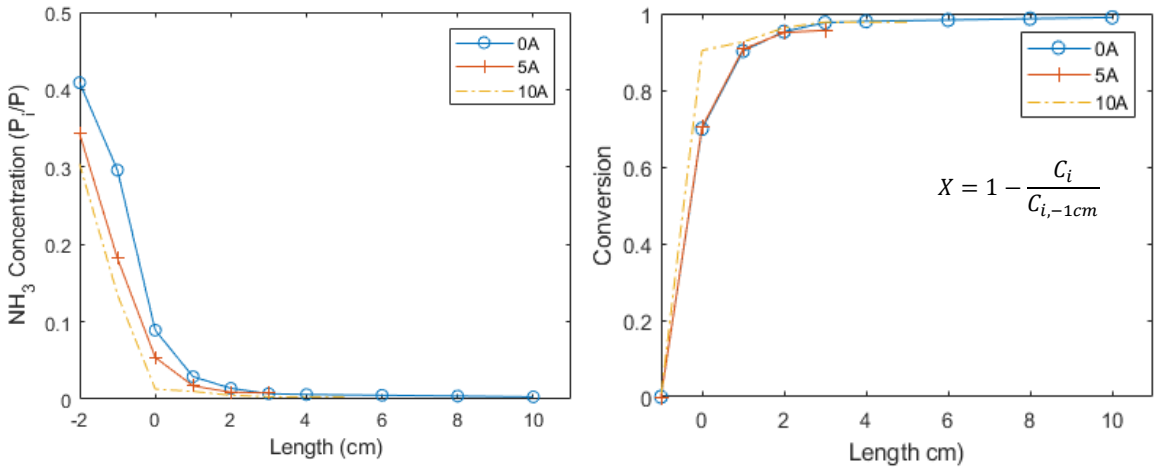

Figure 22: (left) Concentration profiles of ammonia inside *t*-SOFC at 700 ºC and currents of 0A, 5A, and 10A; and (right) the corresponding ammonia conversion. Current density has slight influence to the concentration gradients inside *t*-SOFC. Ammonia conversion is achieved a bit sooner under higher operating current.

It is found that the rate of ammonia consumption increases with the operating current. Complete conversion is expected at 6cm for the current of 0A and 4cm for the current of 10A respectively. It is likely that complete conversion could be achieved at the cell inlet if operating at 15A and above (18A for maximum power).

Additionally, as shown in Figure 23, the hydrogen concentration profiles along the length of the fuel cell is observed and found to correlate nicely with the previous observations.

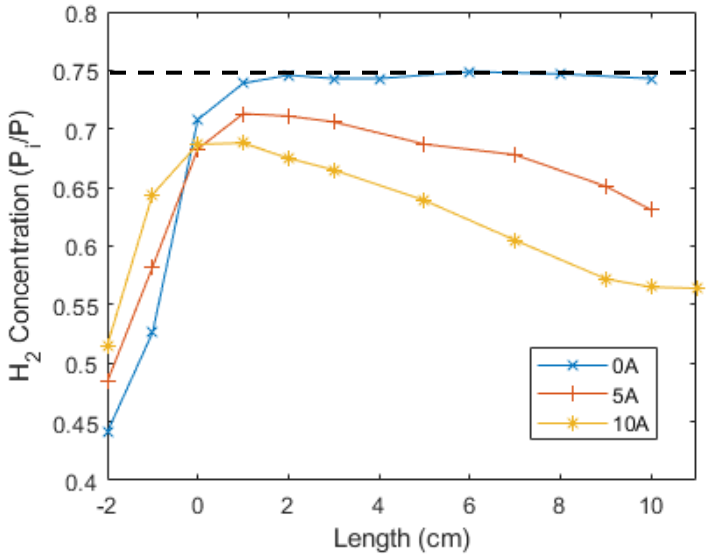

Figure 23: Hydrogen concentration profiles inside *t*-SOFC at 700 ºC and currents of 0A, 5A, and 10A. Hydrogen is rapidly produced within the first 2cm of *t*-SOFC. Hydrogen concentration stabilizes approximately 75% under OCV. When the current is drawn, the rate of hydrogen consumption increases with current density. The stoichiometric limit for hydrogen concentration is at 0.75 (dash line).

Hydrogen is rapidly produced within the first 2cm of the cell. Under OCV, hydrogen concentration stabilizes approximately at 75% which matches with the value when

ammonia is completely converted. When a current is drawn, hydrogen is rapidly generated and gradually consumed along the length of the cell. Faster rate is observed with higher operating current. It should also be noted that the amount of hydrogen being consumed at 10A is less than 30% of the produced hydrogen gas. Clearly, higher current and utilization are possible.

3.4 Durability test and SEM-EDS images

As mentioned previously, ammonia *t*-SOFC not only provides identical performance to an equivalent hydrogen-nitrogen *t*-SOFC but also offers a better durability when compared to those fueled by hydrocarbon fuels. Since ammonia is carbon-free, the premature carbon deposition on the anode surface can be neglected. To further verify this advantage of ammonia-fueled *t*-SOFC, it is of interests to evaluate its durability and anode surface characteristics.

The power generated by the ammonia *t*-SOFC running at 700ºC and a current of 10A, which is equivalent to 23% fuel utilization (U_f) was observed over a period of 22 hours. The decreasing rate of power, or the degradation rate, of -0.000029 W/h was estimated. This value is and consistent with our prior work using the simulated biogas fuel at 900ºC and 23% fuel utilization [11]. The degradation rate observed in ammonia *t*-SOFC is lower than those obtained in prior work by an order of magnitude indicating a more stable performance.

Furthermore, the SEM-EDS images in Figure 24 were collected to show the Ni-YSZ anode surfaces and nickel catalyst distributions of a fresh (top) and a used

(bottom) *t*-SOFCs. The used one was operated with ammonia fuel feed at temperatures above 700ºC approximately for 50 hours. It is observed that the Ni-YSZ cermet surfaces of both cells are in the same condition and no significant fracture is found. Both EDS images do not show sign of catalyst sintering but shows uniform distribution of nickel catalyst on the cermet surfaces. These observations confirm that ammonia *t*-SOFC provides stable performance and good durability.

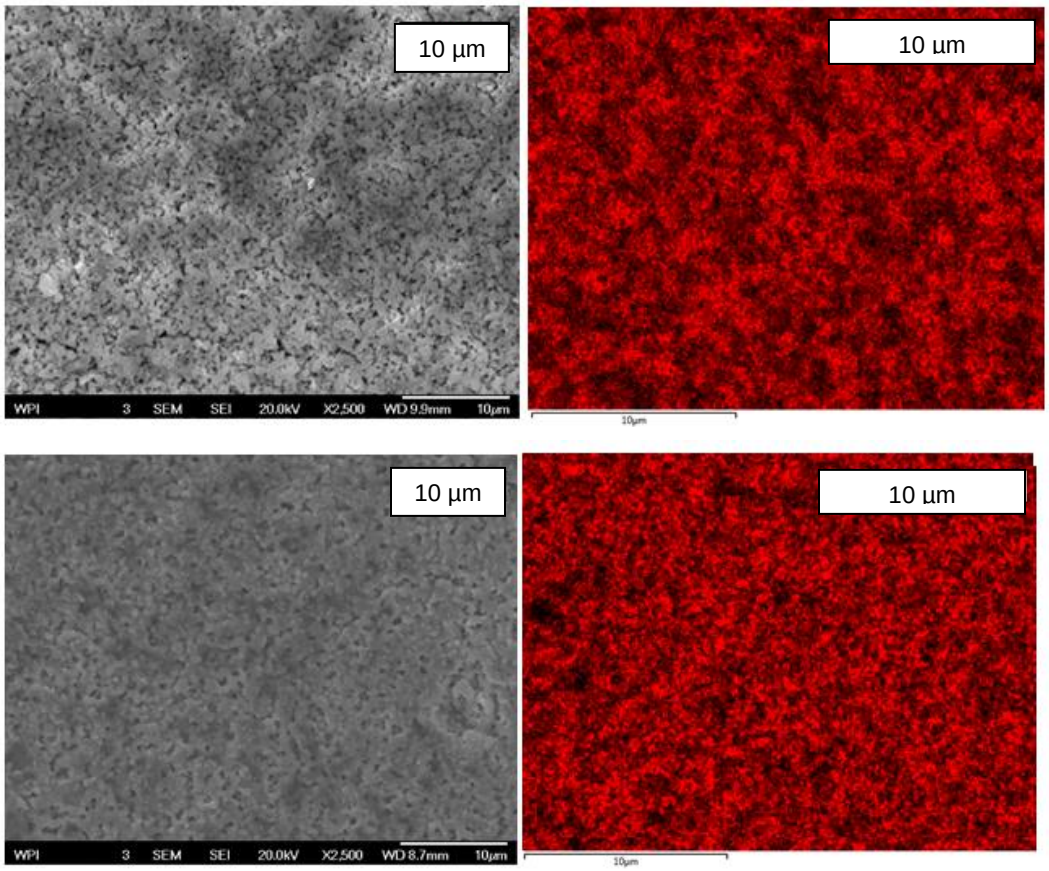

Figure 24: SEM-EDS images of Ni-YSZ cermet surfaces of a fresh (top) and a used (bottom) t-SOFCs. No significant fracture or Ni catalyst sintering is found. EDS images of both samples show uniform distribution of Ni catalyst on cermet surfaces.

Chapter 4

Conclusion and Future Outlook

In this study, the comparison of cell performances obtained at various operating parameters reveals that ammonia-fueled *t*-SOFCs give identical performance to an equivalent hydrogen-fueled *t*-SOFC. With 100 SCCM of ammonia fuel feed, a maximum power of 12.2 W and fuel utilization of 81% are obtained at 800 ºC. The experimental analyses of temperature and concentration profiles confirm that the overall reactions proceed in a two-stage process; 1) endothermic ammonia decomposition and 2) exothermic hydrogen oxidation. Rate of ammonia decomposition is rapid at the inlet of the *t*-SOFC and increases with temperature and operating current density. The cooling effect or heat integration from decomposition reaction provides favorable influences to the temperature and concentration profiles inside *t*-SOFC. However, this cooling effect is most noticeable when the *t*-SOFC is operated at furnace temperature of less than or equal to 700 ºC. This is due to the thermal cracking of ammonia inside a stainless steel tube prior to *t*-SOFC inlet. Complete conversion of ammonia in *t*-SOFC is confirmed at furnace temperature above 600 ºC. The catalytic cracking of ammonia is observed over the nickel anode surface of *t*-SOFC and the apparent activation energy for ammonia decomposition is 82,000 J/mol. The 23-hour stability test and SEM-EDS images of

the fresh and used Ni-YSZ cermet surfaces confirm uniform performance and good durability of *t*-SOFC.

Since ammonia *t*-SOFCs demonstrate beneficial heat integration below 700ºC, future work should include comprehensive study of heat integration and cell performance of intermediate-temperature ammonia-fueled *t*-SOFCs as well as the corresponding degradation rate. In recent work by Baharuddin et al. [35], the LSCF cathode demonstrated excellent performance and compatibility with intermediate-temperature electrolyte. We therefore could expect a higher endothermic contribution and a closer step toward achieving autothermal operation in ammonia *t*-SOFC. Process intensification should look to use axial flow distribution and catalyst gradients to engineer axially uniform reaction flux gradients. Doing so will further prove to maintain operation near the region of maximum performance while maximizing fuel utilization at low temperature, autothermal conditions.

An extension of this technology can be envisioned for flexible-fuel systems. Fuel cells using hydrocarbon fuels as the hydrogen-carriers can operate at increased efficiency and shelf life of using *t*-SOFCs by careful exploitation of the endothermic hydrocarbon reforming. Undesirable carbon deposition, which is typically caused by the cold spots, could also be alleviated by careful design of fuel cell system such that a gradual reaction flux is achieved axially. Additionally, the coupled hydrodynamic and dynamic electrochemical models for performance evaluation of single and stacked *t*-SOFC should be developed to develop next generation reactor geometries. Thorough understanding of fuel cell system and

utilization of carbon-free fuels not only allow a sustainable and efficient power generation but could also lead to a carbon-neutral economy, minimizing anthropogenic climate change.

References

[1] USGCRP Indicator Details | GlobalChange.gov, (n.d.). https://www.globalchange.gov/browse/indicators/indicator-annual-greenhouse-gas-index (accessed April 21, 2019).

[2] Nivaas Sudhan, HYDROGEN ECONOMY – Ré, (n.d.). https://researchandexploration.wordpress.com/2017/05/26/hydrogen-economy/ (accessed April 21, 2019).

[3] C.H. Christensen, T. Johannessen, R.Z. Sørensen, J.K. Nørskov, Towards an ammonia-mediated hydrogen economy ?, Catal. Today. 111 (2006) 140–144. doi:10.1016/j.cattod.2005.10.011.

[4] D.J. Little, M.R. Smith, III, T.W. Hamann, Electrolysis of liquid ammonia for hydrogen generation, Energy Environ. Sci. 8 (2015) 2775–2781. doi:10.1039/C5EE01840D.

[5] A. Klerke, C.H. Christensen, J.K. Nørskov, T. Vegge, Ammonia for hydrogen storage : challenges and opportunities †, J. Mater. Chem. 18 (2008) 2304–2310. doi:10.1039/b720020j.

[6] R.M. Ormerod, Solid oxide fuel cells, Chem. Soc. Rev. 32 (2003) 17–28. doi:10.1039/b105764m.

[7] S.A. Sherif, F. Barbir, T.N. Veziroglu, Wind energy and the hydrogen economy — review of the technology, Sol. Energy. 78 (2005) 647–660.

doi:10.1016/j.solener.2005.01.002.

[8] S. Mekhilef, R. Saidur, A. Safari, Comparative study of different fuel cell technologies, Renew. Sustain. Energy Rev. 16 (2012) 981–989. doi:10.1016/j.rser.2011.09.020.

[9] S.C. Singhal, Advances in solid oxide fuel cell technology, Solid State Ionics. 135 (2000) 305–313.

[10] W. Bujalski, C.M. Dikwal, K. Kendall, Cycling of three solid oxide fuel cell types, J. Power Sources. 171 (2007) 96–100. doi:10.1016/j.jpowsour.2007.01.029.

[11] C.M. Jones, J. Persky, R. Datta, Exploring Conditions That Enhance Durability and Performance of a Tubular Solid Oxide Fuel Cell Fed with Simulated Biogas, (2017) 12875–12892. doi:10.1021/acs.energyfuels.7b02362.

[12] Beau Jackson, European Commission backs 3D printed clean energy project Cell3Ditor - 3D Printing Industry, (n.d.). https://3dprintingindustry.com/news/european-commission-backs-3d-printed-clean-energy-project-cell3ditor-119467/ (accessed April 21, 2019).

[13] M. Ni, D.Y.C. Leung, M.K.H. Leung, Mathematical modeling of ammonia-fed solid oxide fuel cells with different electrolytes, Int. J. Hydrogen Energy. 33 (2008) 5765–5772. doi:10.1016/j.ijhydene.2008.07.021.

[14] M. Ni, D.Y.C. Leung, M.K.H. Leung, An improved electrochemical model for

the NH 3 fed proton conducting solid oxide fuel cells at intermediate temperatures, J. Power Sources. 185 (2008) 233–240. doi:10.1016/j.jpowsour.2008.07.023.

[15] A. Fuerte, R.X. Valenzuela, M.J. Escudero, L. Daza, Ammonia as efficient fuel for SOFC, J. Power Sources. 192 (2009) 170–174. doi:10.1016/j.jpowsour.2008.11.037.

[16] C. Zamfirescu, I. Dincer, Using ammonia as a sustainable fuel, J. Power Sources. 185 (2008) 459–465. doi:10.1016/j.jpowsour.2008.02.097.

[17] S. Farhad, F. Hamdullahpur, Conceptual design of a novel ammonia-fuelled portable solid oxide fuel cell system, J. Power Sources. 195 (2010) 3084–3090. doi:10.1016/j.jpowsour.2009.11.115.

[18] J.J. Mackenzie, W.H. Avery, Ammonia fuel: the key to hydrogen-based transportation, in: Energy Convers. Eng. Conf., 1996: pp. 1761–1766.

[19] A. Ahmed, N. Radenahmad, Q. Cheok, S. Shams, J.H. Kim, A.K. Azad, Ammonia-fed fuel cells : a comprehensive review, Renew. Sustain. Energy Rev. 60 (2016) 822–835. doi:10.1016/j.rser.2016.01.120.

[20] A. Wojcik, H. Middleton, I. Damopoulos, J. Van herle, Ammonia as a fuel in solid oxide fuel cells, J. Power Sources. 118 (2003) 342–348. doi:10.1016/S0378-7753(03)00083-1.

[21] J. Staniforth, R.M. Ormerod, Clean destruction of waste ammonia with

consummate production of electrical power within a solid oxide fuel cell system, Green Chem. 5 (2003) 606–609. doi:10.1039/b307396n.

[22] Q. Ma, R. Peng, Y. Lin, J. Gao, G. Meng, A high-performance ammonia-fueled solid oxide fuel cell, J. Power Sources. 161 (2006) 95–98. doi:10.1016/j.jpowsour.2006.04.099.

[23] N.J.J. Dekker, Highly Efficient Conversion of Ammonia in Electricity by Solid Oxide Fuel Cells, J. Fuel Cell Sci. Technol. 3 (2006) 499–502. doi:10.1115/1.2349536.

[24] M. Ni, M.K.H. Leung, D.Y.C. Leung, Ammonia-fed solid oxide fuel cells for power generation — A review, Int. J. Energy Res. 33 (2009) 943–959. doi:10.1002/er.

[25] G. Cinti, U. Desideri, D. Penchini, G. Discepoli, Experimental Analysis of SOFC Fuelled by Ammonia, Fuel Cells. (2014) 221–230. doi:10.1002/fuce.201300276.

[26] J. Yang, A.F. Salem Molouk, T. Okanishi, H. Muroyama, T. Matsui, K. Eguchi, Electrochemical and Catalytic Properties of Ni/BaCe0.75Y0.25O3−δ Anode for Direct Ammonia-Fueled Solid Oxide Fuel Cells, ACS Appl. Mater. Interfaces. 7 (2015) 7406–7412. doi:10.1021/acsami.5b01048.

[27] J. Yang, A. Fathi, S. Molouk, T. Okanishi, H. Muroyama, T. Matsui, K. Eguchi, A Stability Study of Ni / Yttria-Stabilized Zirconia Anode for Direct Ammonia Solid Oxide Fuel Cells, ACS Appl. Mater. Interfaces. 7 (2015) 28701–28707.

doi:10.1021/acsami.5b11122.

[28] Q. Ma, R. Peng, L. Tian, G. Meng, Direct utilization of ammonia in intermediate-temperature solid oxide fuel cells, Electrochem. Commun. 8 (2006) 1791–1795. doi:10.1016/j.elecom.2006.08.012.

[29] P.G. Smirniotis, D.A. Peña, B.S. Uphade, Low-Temperature Selective Catalytic Reduction (SCR) of NO with NH3 by Using Mn, Cr, and Cu Oxides Supported on Hombikat TiO2, Angew. Chemie Int. Ed. 40 (2001) 2479–2482. doi:10.1002/1521-3773(20010702)40:13<2479::AID-ANIE2479>3.0.CO;2-7.

[30] X. Mou, B. Zhang, Y. Li, L. Yao, X. Wei, D.S. Su, W. Shen, Rod-Shaped Fe_2O_3 as an Efficient Catalyst for the Selective Reduction of Nitrogen Oxide by Ammonia, Angew. Chemie Int. Ed. 51 (2012) 2989–2993. doi:10.1002/anie.201107113.

[31] G. Cinti, G. Discepoli, E. Sisani, U. Desideri, SOFC operating with ammonia : Stack test and system analysis, Int. J. Hydrogen Energy. 41 (2016) 13583–13590. doi:10.1016/j.ijhydene.2016.06.070.

[32] M. Ni, Thermo-electrochemical modeling of ammonia-fueled solid oxide fuel cells considering ammonia thermal decomposition in the anode, Int. J. Hydrogen Energy. 36 (2011) 3153–3166. doi:10.1016/j.ijhydene.2010.11.100.

[33] C. Spiegel, Polarization Curves, Fuel Cell Basics. (2017). https://www.fuelcellstore.com/blog-section/polarization-curves (accessed April 25, 2019).

[34] T. V Choudhary, C. Sivadinarayana, D.W. Goodman, Catalytic ammonia decomposition : CO x -free hydrogen production for fuel cell applications, Catal. Letters. 72 (2001) 197–201.

[35] N.A. Baharuddin, H.A. Rahman, A. Muchtar, Development of lanthanum strontium cobalt ferrite composite cathodes for intermediate- to low-temperature solid oxide fuel cells *, 14 (2013) 11–24. doi:10.1631/jzus.A1200134.

Appendix A

Supporting Information

A.1 Polarization curves

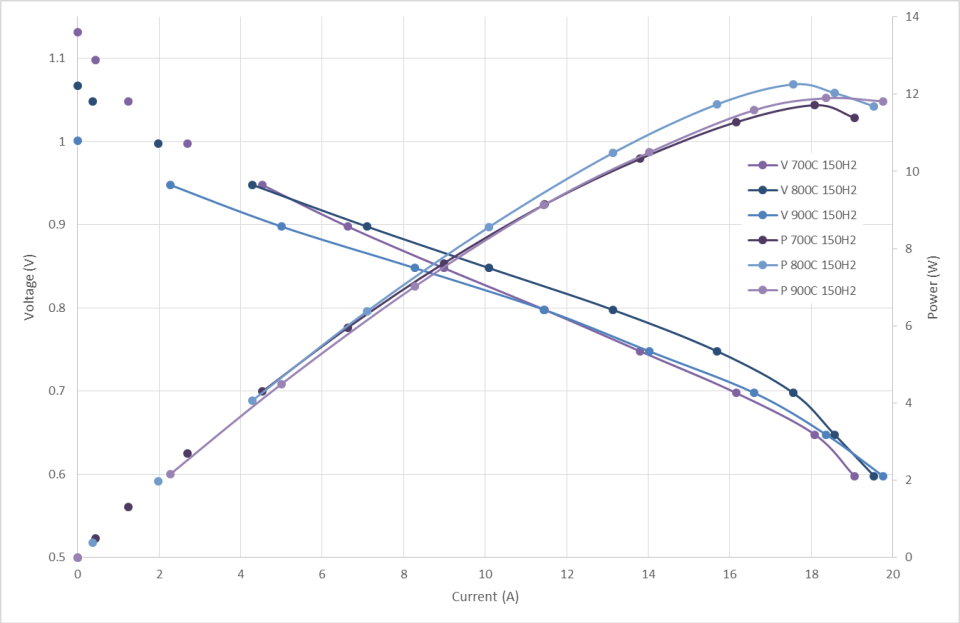

Figure A.1: Polarization curves for 150 SCCM H_2

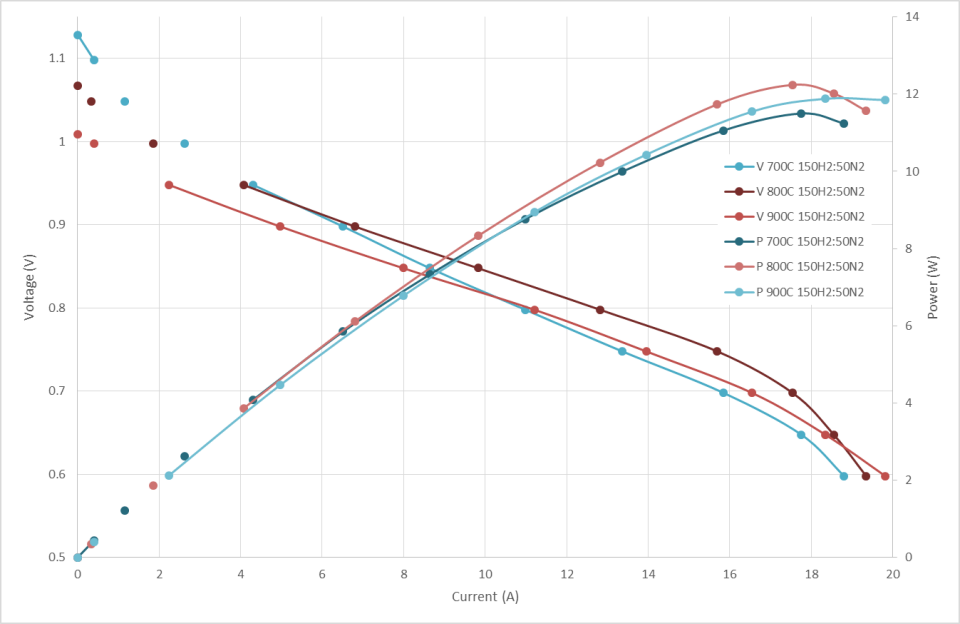

Figure A.2: Polarization curves for 150 SCCM H_2: 50 SCCM N_2

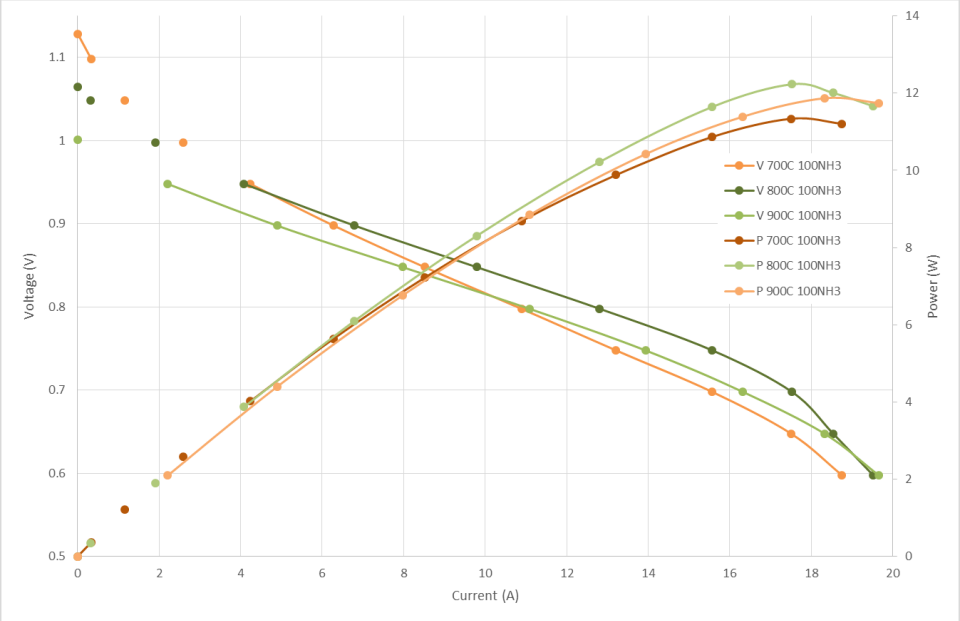

Figure A.3: Polarization curves for 100 SCCM NH_3

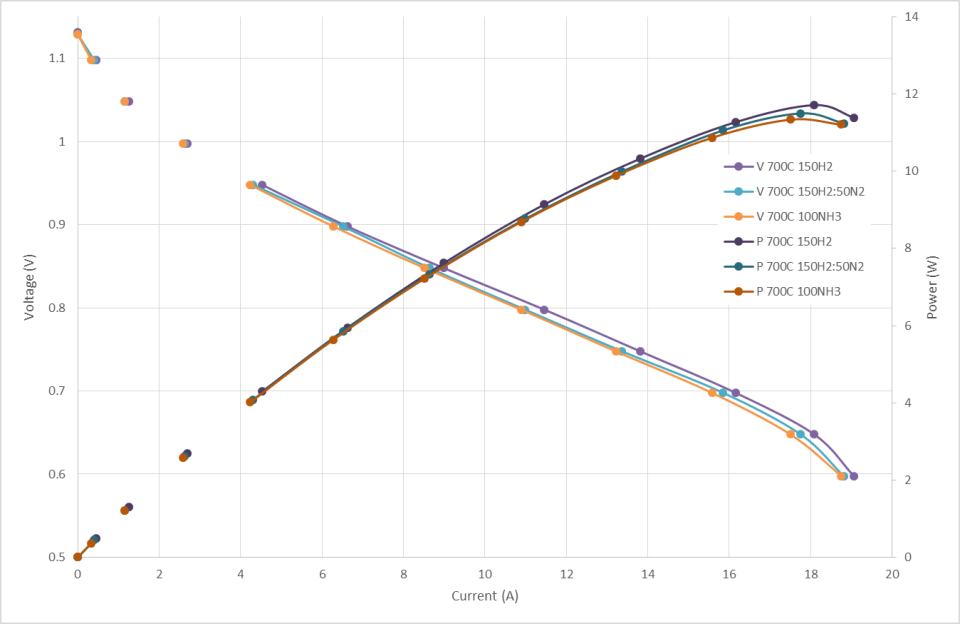

Figure A.4: Polarization curves at 700 ºC for all fuel compositions

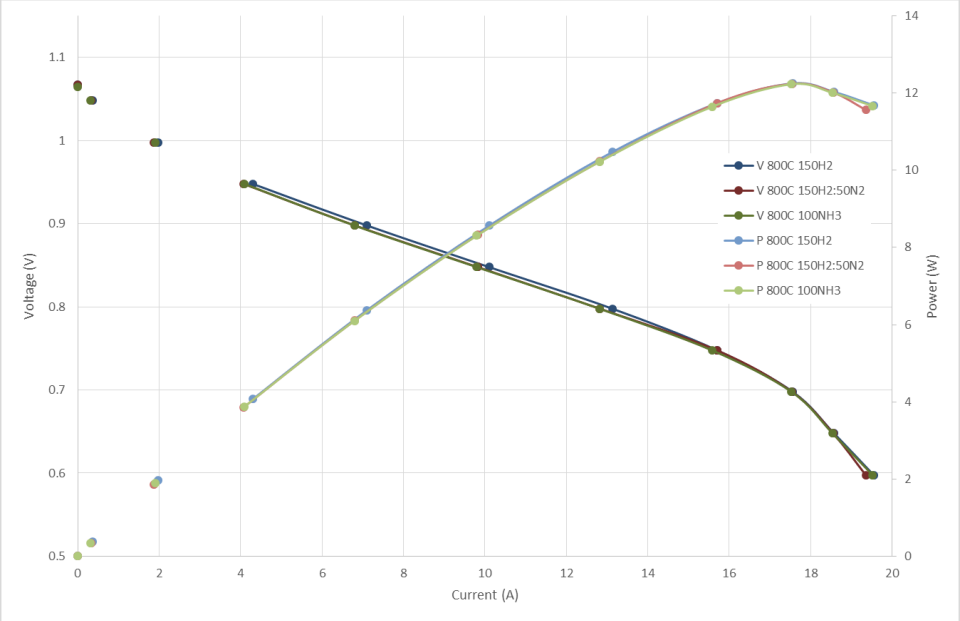

Figure A.5: Polarization curves at 800 ºC for all fuel compositions

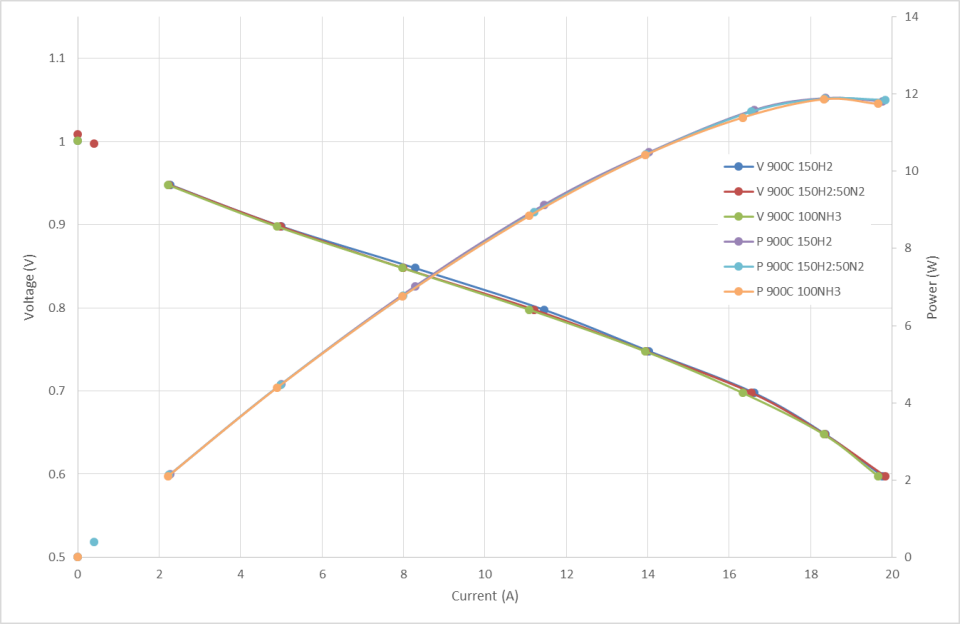

Figure A.6: Polarization curves at 900 ºC for all fuel compositions

A.2 Temperature Profile in Furnace

Temperature gradients within the well-insulated furnace existed. Heating peaks in the middle of the furnace and lower temperatures at the two ends of the furnace were observed. Temperature profiling at furnace temperatures of 700ºC and 900ºC were monitored and collected in order to locate the best spot for *t*-SOFC placement within the furnace. It is found that the optimal placement of t-SOFC should be 9.5cm to 22.5cm from the inlet of the furnace.

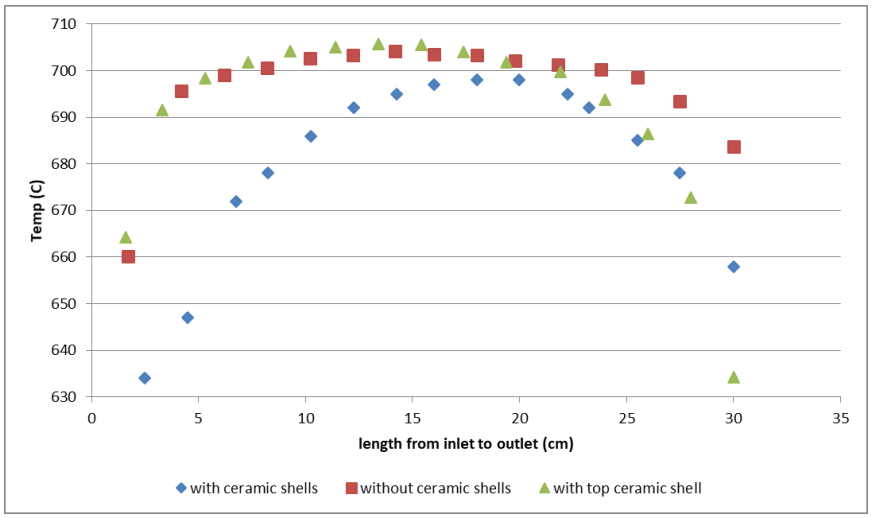

Figure A.7: Temperature profile of 700ºC furnace

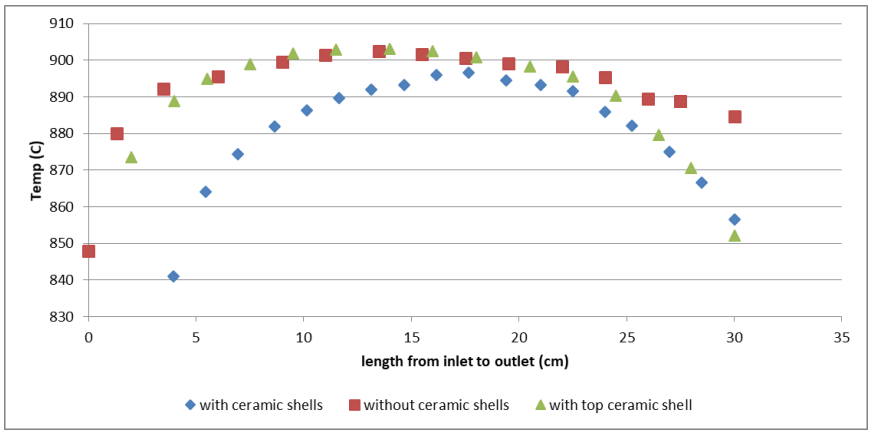

Figure A.8: Temperature profile of 900ºC furnace

A.3 Temperature Profiles of *t*-SOFC

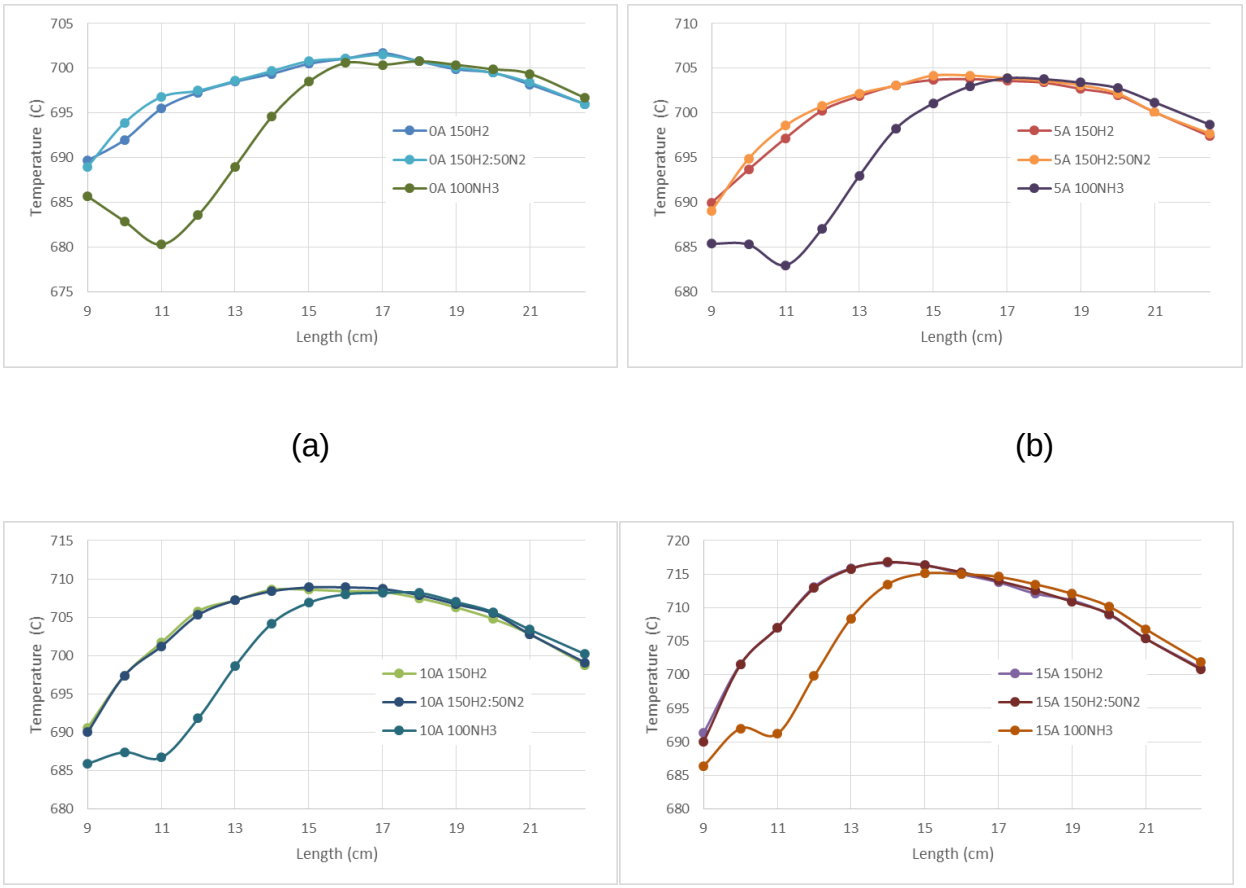

Figure A.9: Temperature profiles for 3 fuel gases at (a) 0A, (b) 5A, (c) 10A, and (d) 15A. Furnace temperature of 700 ºC

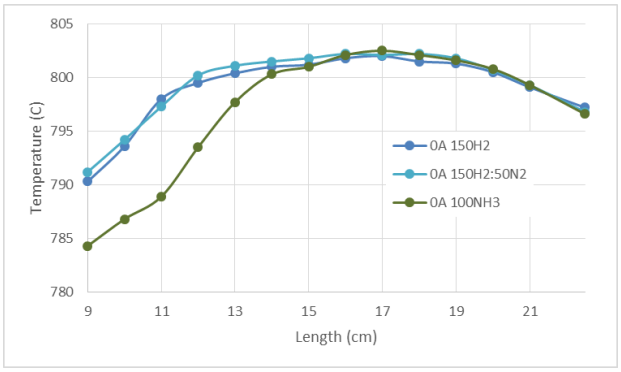

(a)

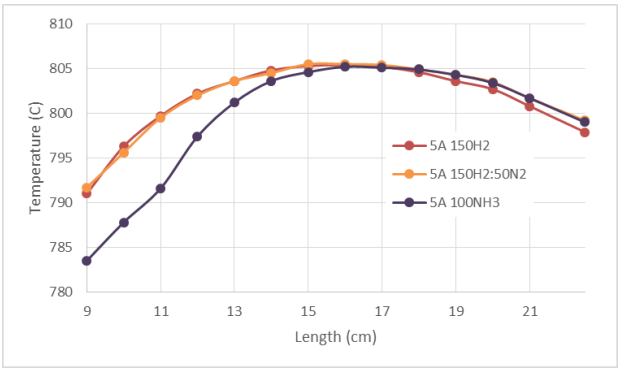

(b)

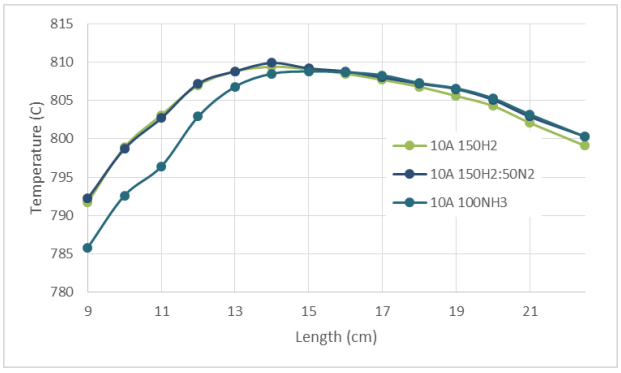

(c)

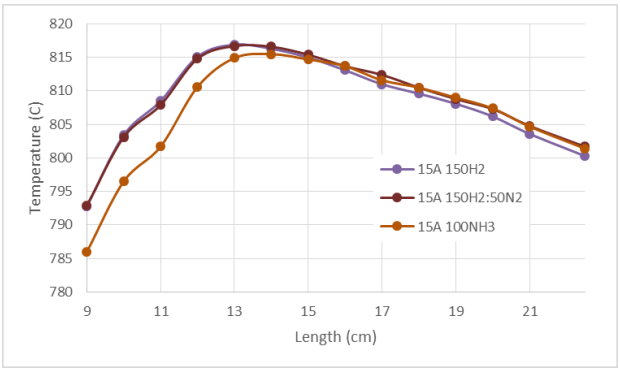

(d)

Figure A.10: Temperature profiles for 3 fuel gases at (a) 0A, (b) 5A, (c) 10A, and (d) 15A. Furnace temperature of 800 ºC

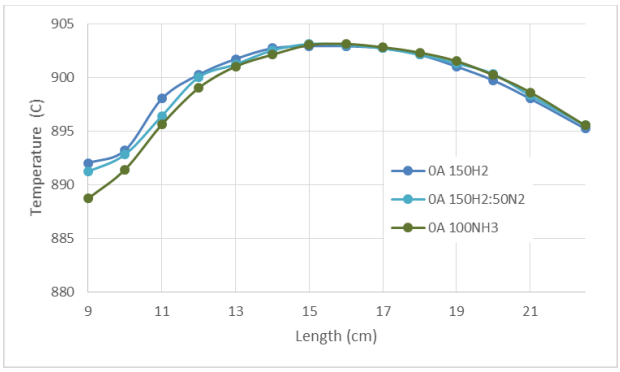

(a)

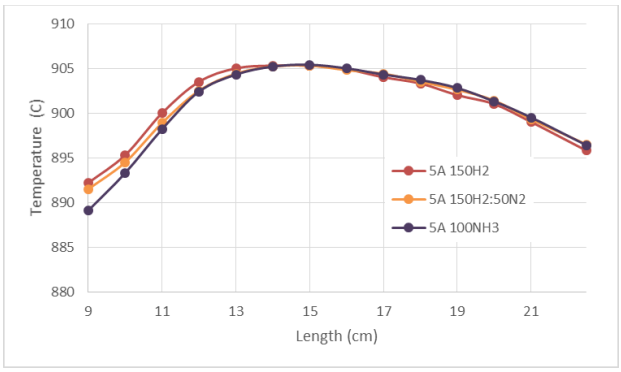

(b)

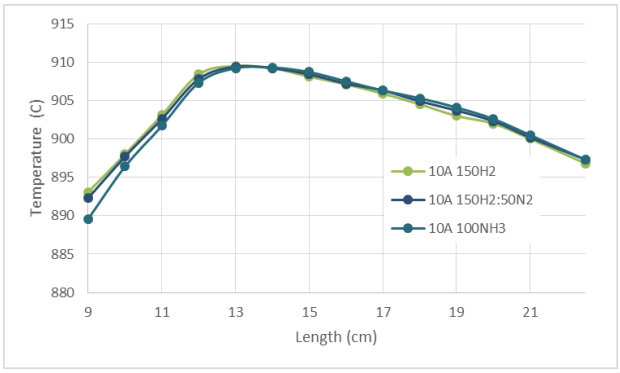

(c)

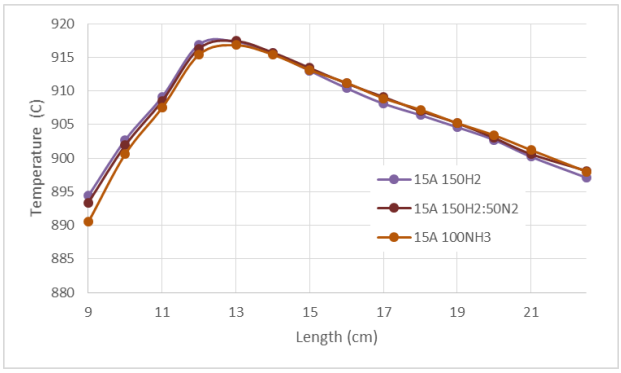

(d)

Figure A.11: Temperature profiles for 3 fuel gases at (a) 0A, (b) 5A, (c) 10A, and (d) 15A. Furnace temperature of 900 ºC

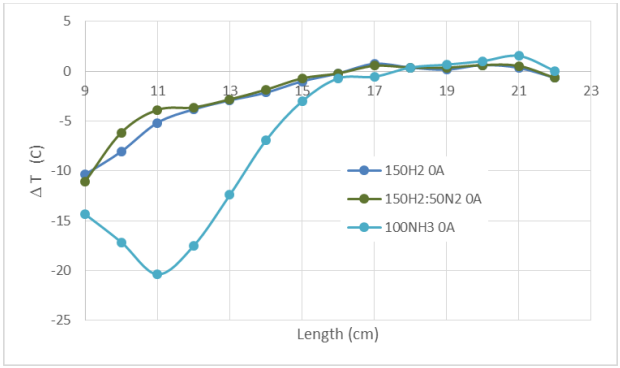

(a)

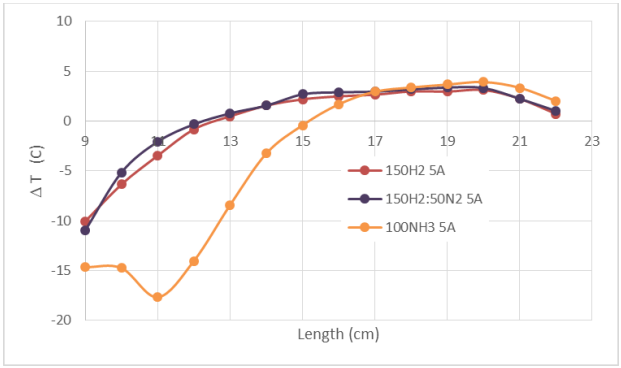

(b)

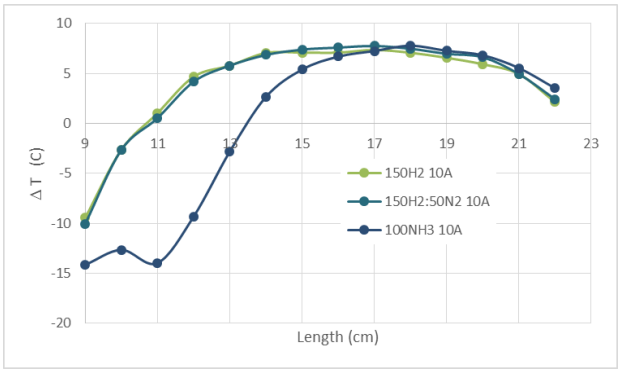

(c)

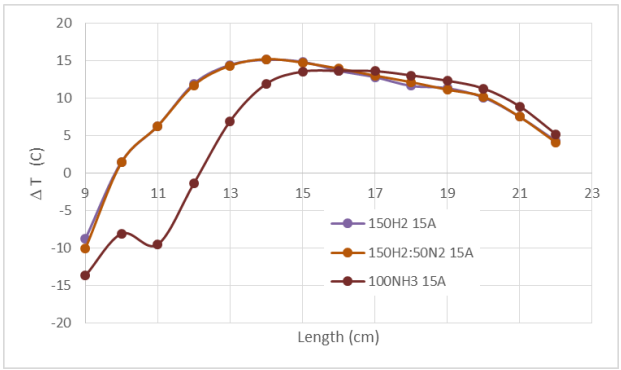

(d)

Figure A.12: Temperature differences (a) 0A, (b) 5A, (c) 10A, and (d) 15A.
Furnace temperature of 700 ºC

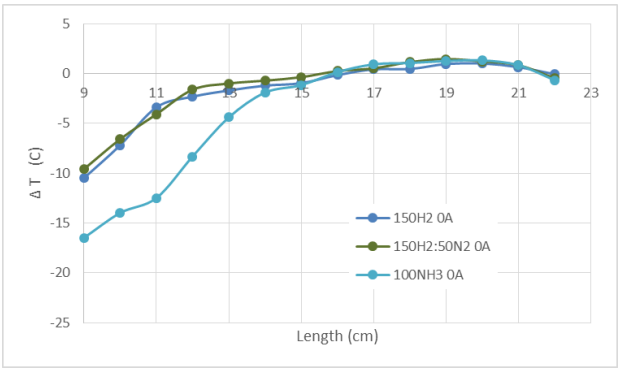

(a)

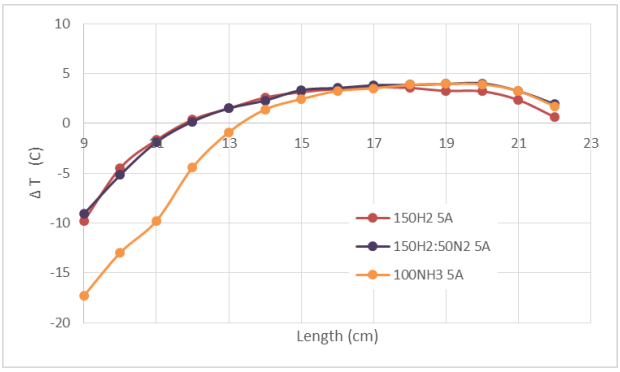

(b)

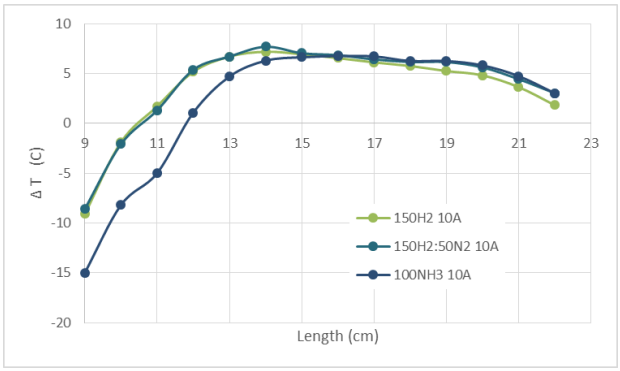

(c)

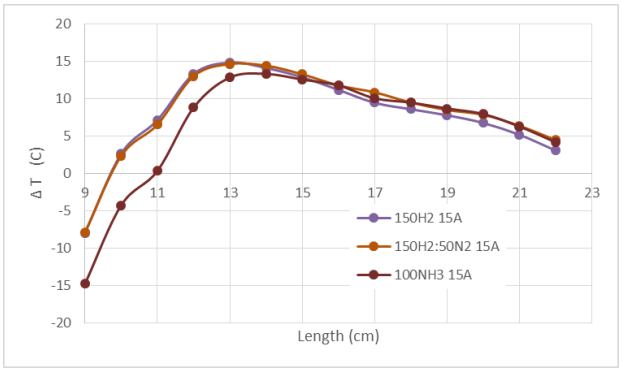

(d)

Figure A.13: Temperature differences (a) 0A, (b) 5A, (c) 10A, and (d) 15A.
Furnace temperature of 800 ºC

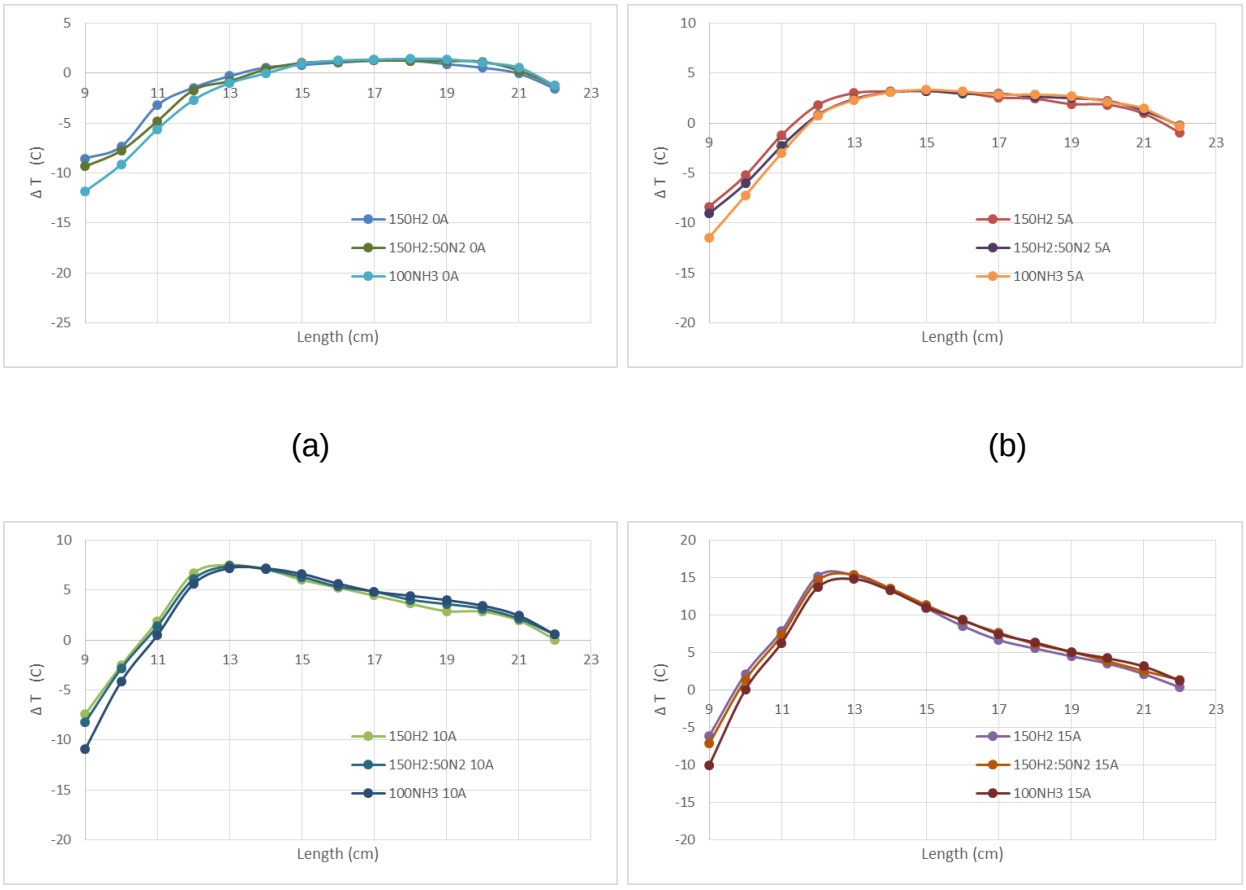

(a) (b)

(c) (d)

Figure A.14: Temperature differences (a) 0A, (b) 5A, (c) 10A, and (d) 15A. Furnace temperature of 900 ºC

A.4 Concentration Profiles of *t*-SOFC

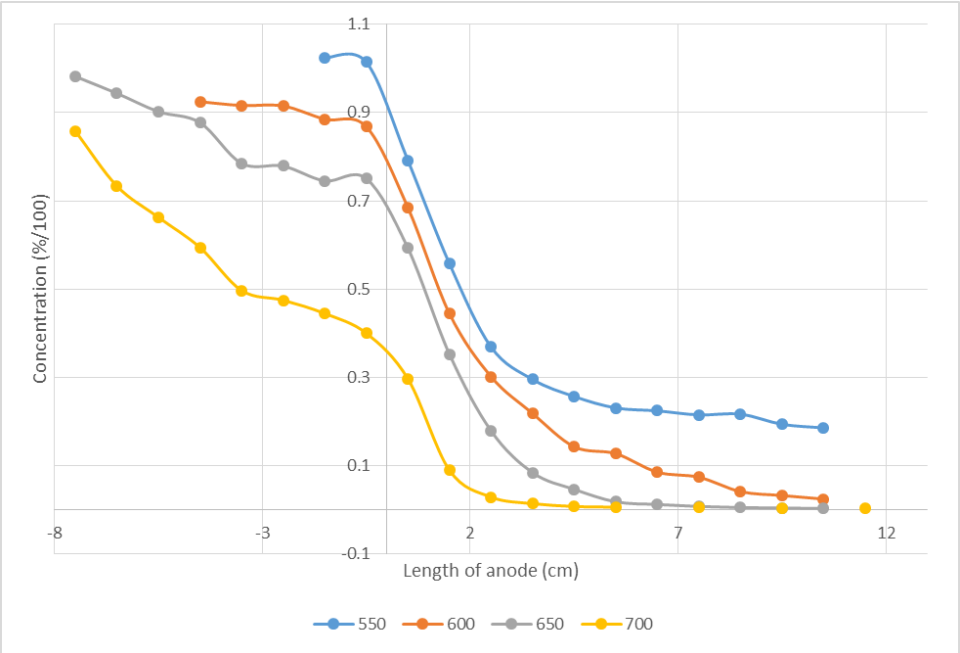

Figure A.15: NH3 Concentration gradients at OCV and different temperatures

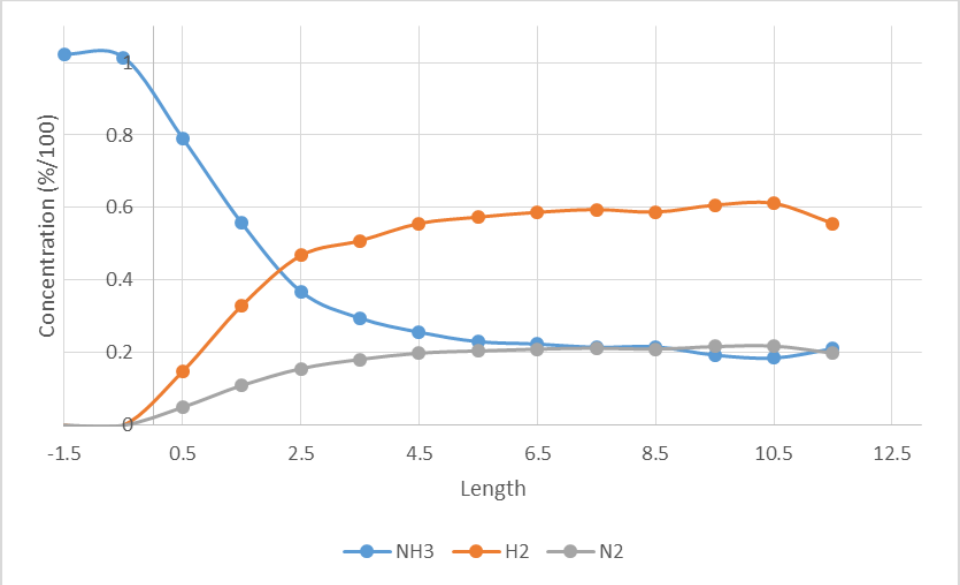

Figure A.16: Concentration gradients of three gases at 550C, 0A.

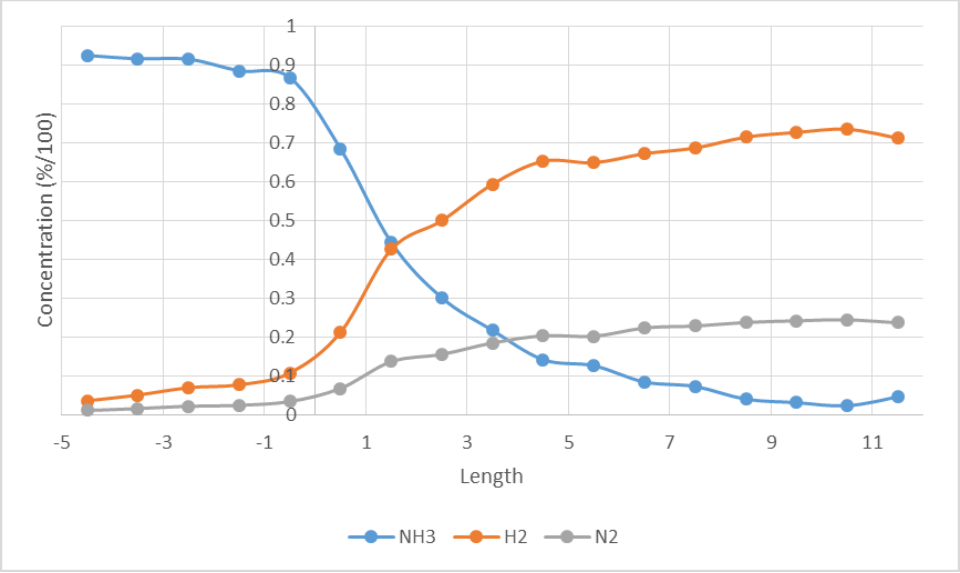

Figure A.17: Concentration gradients of three gases at 600C, 0A.

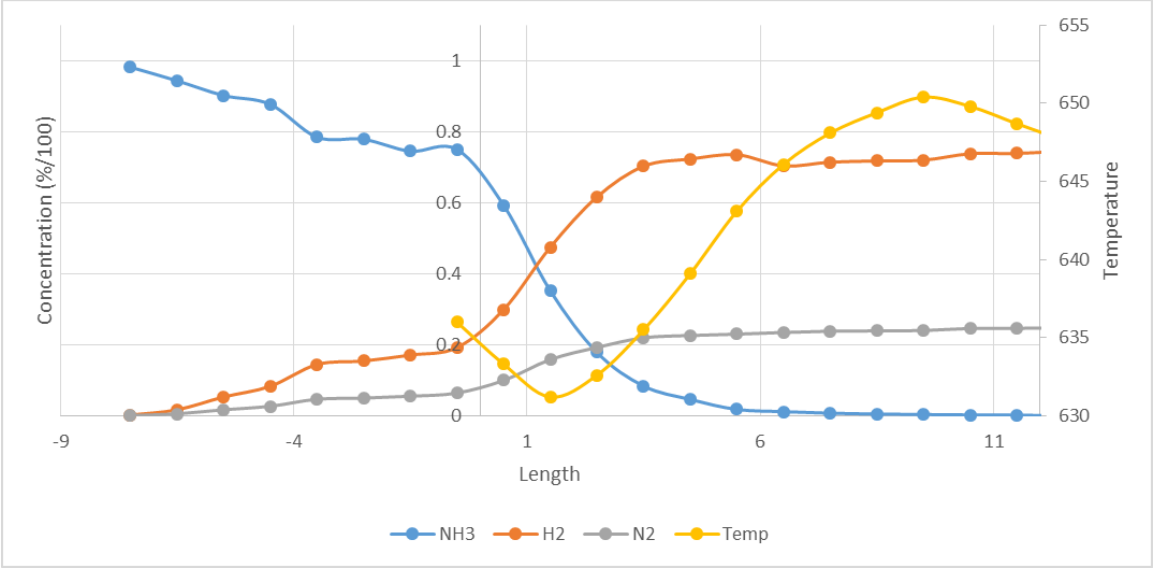

Figure A.18: Concentration gradients of three gases and a temperature profile at 650C, 0A.

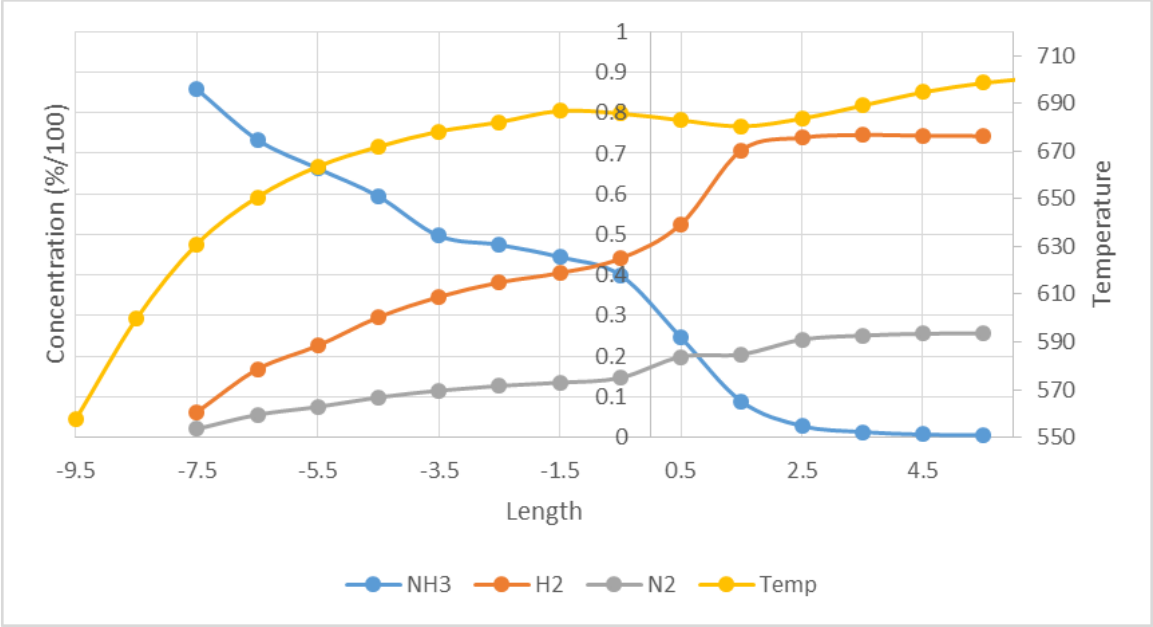

Figure A.19: Concentration gradients of three gases and a temperature profile at 700C, 0A.

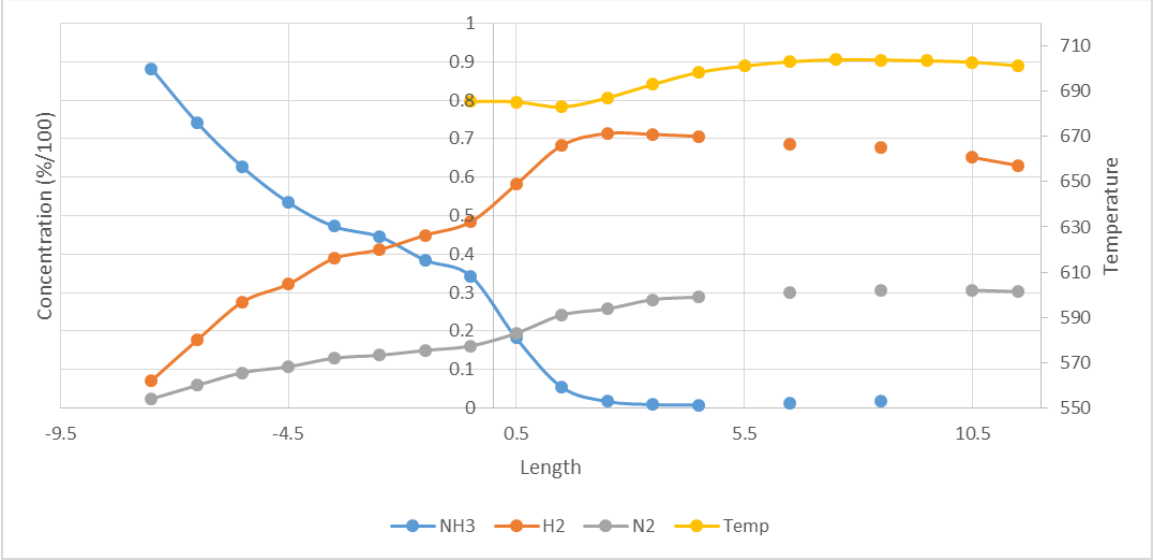

Figure A.20: Concentration gradients of three gases and a temperature profile at 700C, 5A.

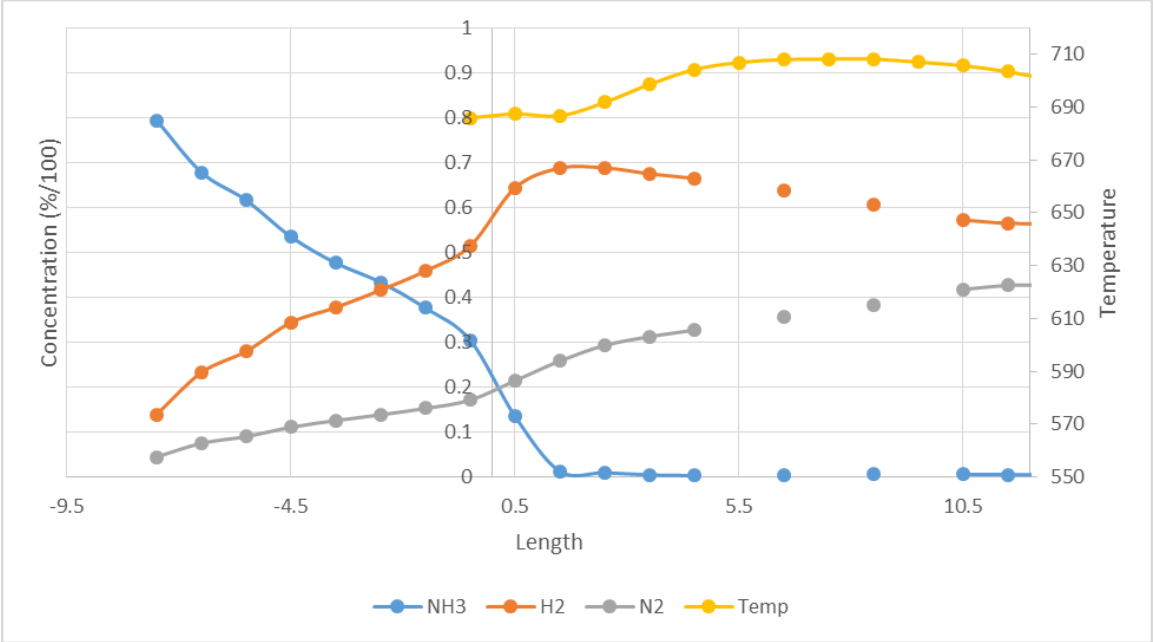

Figure A.21: Concentration gradients of three gases and a temperature profile at 700C, 10A.

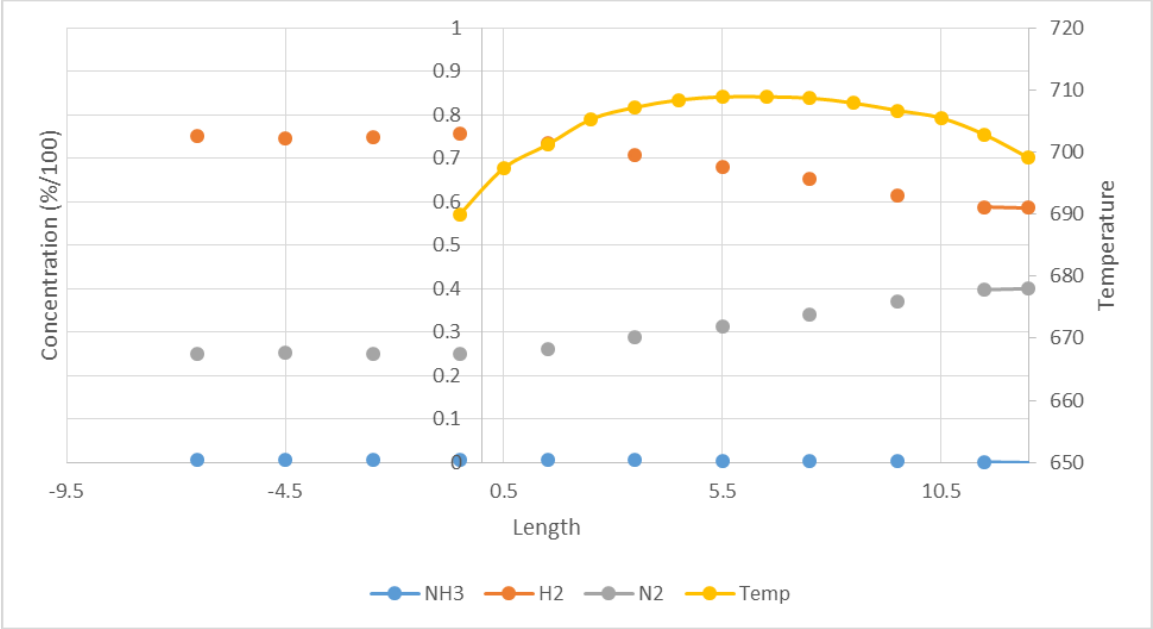

Figure A.22: Concentration gradients of three gases and a temperature profile at 700C, 10A. $3H_2$:N_2 feed